Treatment with IFB-088 improves neuropathy in CMT1A and CMT1B mice

Yunhong Bai,[1] Caroline Treins,[2] Vera G. Volpi,[3] Cristina Scapin,[3] Cinzia Ferri,[3] Rosa Mastrangelo,[3] Thierry Touvier,[3] Francesca Florio,[3] Francesca Bianchi,[4] Ubaldo Del Carro,[4] Frank F. Baas,[5] David Wang,[1] Pierre Miniou,[2] Philippe Guedat,[3] Michael E. Shy[1,†] and Maurizio D'Antonio[3,†]

[†] **These authors contributed equally to the manuscript**

Author affiliations:

[1] Department of Neurology, Carver College of Medicine, University of Iowa, Iowa City, Iowa, IA 52242, USA

[2] InFlectis BioScience, 44300 Nantes, France

[3] Division of Genetics and Cell Biology, San Raffaele Scientific Institute DIBIT, 20132 Milano, Italy

[4] Division of Neuroscience, San Raffaele Scientific Institute DIBIT, 20132 Milano, Italy

[5] Department of Clinical Genetics, Leiden University Medical Center, Leiden, The Netherlands

Author Emails:

Yunhong Bai yunhong-bai@uiowa.edu

Caroline Treins carolinetreins@inflectisbioscience.com

Vera G Volpi volpi.veragiulia@gmail.com

Cristina Scapin scapin33@gmail.com

Cinzia Ferri ferri.cinzia@hsr.it

Rosa Mastrangelo mastrangelo.rosa@hsr.it

Thierry Touvier touvier.thierry@hsr.it

Francesca Florio florio.francesca@hsr.it

Francesca Bianchi bianchi.francesca@hsr.it

Ubaldo Del Carro delcarro.ubaldo@hsr.it

Frank F Baas F.Baas@lumc.nl

David Wang david.wang2@uhhospitals.org

Pierre Miniou pierreminiou@inflectisbioscience.com

Philippe Guedat philippeguedat@inflectisbioscience.com

Michael E Shy michael-shy@uiowa.edu

Maurizio D'Antonio dantonio.maurizio@hsr.it

Corresponding author: Maurizio D'Antonio, PhD, dantonio.maurizio@hsr.it

Abstract

Charcot Marie Tooth diseases type 1A (CMT1A), caused by duplication of Peripheral Myelin Protein 22 (*PMP22*) gene, and CMT1B, caused by mutations in myelin protein zero (*MPZ*) gene are the two most common forms of demyelinating CMT (CMT1) and no treatments are available for either. Prior studies of the *Mpz*Ser63del mouse model of CMT1B have demonstrated that protein misfolding, endoplasmic reticulum (ER) retention and activation of the unfolded protein

response (UPR) contributed to the neuropathy. Heterozygous patients with an arginine to cysteine mutation in MPZ (*MPZ*R98C) develop a severe infantile form of CMT1B which is modeled by *Mpz*R98C/+ mice that also show ER-stress and an activated UPR. C3-PMP22 mice are considered to effectively model CMT1A. Altered proteostasis, ER-stress and activation of the UPR have been demonstrated in mice carrying *Pmp22* mutations. To determine whether enabling the ER-stress/UPR and readjusting protein homeostasis would effectively treat these models of CMT1B and CMT1A we administered Sephin1/IFB-088/icerguestat, a UPR modulator which showed efficacy in the MpzS63del model of CMT1B, to heterozygous *Mpz*R98C and C3-PMP22 mice. Mice were analyzed by behavioral, neurophysiological, morphological and biochemical measures. Both *Mpz*R98C/+ and C3-PMP22 mice improved in motor function and neurophysiology. Myelination, as demonstrated by g-ratios and myelin thickness, improved in CMT1B and CMT1A mice and markers of UPR activation returned towards wild type values. Taken together our results demonstrate the capability of IFB-088 to treat a second mouse model of CMT1B and a mouse model of CMT1A, the most common form of CMT. Given the recent benefits of IFB-088 treatment in Amyotrophic Lateral Sclerosis and Multiple Sclerosis animal models, these data demonstrate its potential in managing UPR and ER-stress for multiple mutations in CMT1 as well as in other neurodegenerative diseases.

Keywords: Charcot Marie Tooth; neuropathy; proteostasis; UPR; IFB-088

Introduction

Charcot Marie Tooth (CMT) disease refers to heritable peripheral neuropathies, which are the most common genetic neuromuscular diseases, affecting 1:2500 individuals [60]. Autosomal dominant (AD) inheritance is the most common, followed by X-linked and autosomal recessive (AR) forms. Most forms of CMT are demyelinating while approximately one-third appear to be primary axonal disorders [18, 43]. CMT1A is the most common form, affecting approximately half of all patients with CMT [18], and is caused by a 1.4Mb duplication within chromosome 17p11.2, in the region containing the peripheral myelin protein 22 (*PMP22)* gene [39, 63]. CMT1B (caused by mutations in myelin protein zero (*MPZ)* gene, encoding for P0 protein) [26] is the second most frequent AD demyelinating form, encompassing around 5% of CMT cases [18]. At present there are no effective treatments to slow progression or improve neuropathy in patients with CMT1A or CMT1B.

80% of newly synthesized PMP22 is rapidly degraded by the proteasome under normal conditions, with only 20% reaching the cell surface or myelin sheath [48]. Whether this ratio is altered when PMP22 is over-expressed in CMT1A is unknown. Ordinarily, the maintenance of correct protein homeostasis is tightly controlled by protein quality control mechanisms [1]. The elevated protein expression associated with *PMP22* trisomy, in conjunction with the instability of the PMP22 protein, impose a heavy burden on the endoplasmic reticulum (ER) protein quality control (ERQC) mechanisms [17, 35, 45, 57] . When these control mechanisms fail, stress responses are activated leading to protein-kinase RNA-like endoplasmic reticulum kinase (PERK) (one of the unfolded protein response (UPR) sensors) mediated phosphorylation of the alpha subunit of the eukaryotic translation initiation factor 2 (eIF2α)[25]. This phosphorylation causes an attenuation of global protein synthesis which reduces protein overload in the ER while

allowing the translation of selected genes supporting stress recovery [38]. The extent to which these responses are activated in CMT1A is unclear, though there have been studies suggesting UPR activation in a CMT1A mouse model carrying seven copies of the human *PMP22* gene, the C22 mouse, which shows a severe dysmyelinating neuropathy [23], and in Trembler J (Tr^J) mice [46], which are caused by a missense mutation in *Pmp22* [33].

Over 200 different mutations in *MPZ* cause neuropathy (http://hihg.med.miami.edu/code/http/cmt/public_html/index.html#/) and the disease mechanisms are largely unknown. One group of mutations presents clinically in infancy or early childhood, with very slow nerve conduction velocities (NCV), and dysmyelination morphologically. Another group of *MPZ* mutations does not present clinically until adulthood, with near normal NCV, and axonal damage but minimal demyelination morphologically (sometimes called CMT2I or CMT2J) [55]. Several *MPZ* mutations in these groups have been shown *in vitro* to cause the accumulation of the mutant protein within the ER, where it triggered ER stress and activated the UPR. These included *Mpz* S51ΔW57 [21], 506delT and 550del3insG [4, 32]. Moreover, two mouse models of CMT1B, the *Mpz*Ser63del and *Mpz*R98C mice [53, 56], demonstrated ER retention of the mutant protein and a canonical UPR. The compound IFB-088 (icerguastat, also known as sephin1) was developed to prolong protein translation attenuation in response to stress by inhibiting eIF2α dephosphorylation to allow cells to restore cellular homeostasis [12]. Oral treatment with IFB-088 largely prevented the molecular, motor and morphological abnormalities of the neuropathy of *Mpz*Ser63del mice [12]. Whether treatment with IFB-088 is effective for only the Ser63del *MPZ* mutation is not known. This is an important question perhaps since as many as 40% of *MPZ* mutations have been recently shown to activate components of the UPR [4]. Accordingly, we elected to treat *Mpz*R98C/+ mice with IFB-088.

We also hypothesized that IFB-088 may have effects on CMT1A, because of the highly metastable nature of PMP22 and because of UPR activity in C22 and Tr^{J} mice [23, 33]. We therefore chose to use IFB-088 to treat the C3-PMP22 mouse model of CMT1A. C3-PMP22 mice, which carry 3-4 copies of the human *PMP22* gene, develop a slowly progressive dysmyelinating peripheral neuropathy that is thought to be an appropriate model of CMT1A [15, 65]. Both CMT1B and CMT1A models were treated IFB-088, and evaluated by behavioral, neurophysiological, morphological and biochemical analysis.

Materials and methods

Myelinating DRG explant cultures

Dorsal-root-ganglia (DRG) were dissected from embryos at embryonic day 13.5 (E13.5) and plated singularly on collagen-coated coverslips as previously described [62]. Myelination was induced with 50 µg/ml ascorbic acid (Sigma Aldrich). Treatment with IFB-088 at the indicated concentration was applied for 2-week in parallel to the induction of myelination. Samples were then fixed and rat anti-MBP (1/5) [11] and rabbit anti-NF-H (1/1000, EMD Millipore) primary antibodies were added o/n at 4°C. The following day, DRGs were washed and FITC- or TRITC-conjugated secondary antibodies (1:200, Cappel) were added for 1h at room temperature. Specimen were incubated with DAPI (1:1000, SIGMA) and mounted with VectaShield (Vector Laboratories). 8-10 images were taken from each DRG using a fluorescence microscope (Leica DM5000) with a 10x objective, and the number of MBP+ internodes in each image was counted.

Animal models

All experiments involving animals were performed in accord with experimental protocols approved by the San Raffaele Scientific Institute and the University of Iowa Animal Care and Use Committee. *Mpz*S63del transgenic mice [70] and *Mpz*R98C/+ knock-in mice [56] were maintained on the FVB/N background. C3-PMP22 transgenic mice [65] were obtained from the Amsterdam University Medical Center, Amsterdam, the Netherland. They were maintained on a C57BL/6J background. C3-PMP22 cohorts for this study were generated via *in vitro* fertilization following the protocol from the European Mouse Mutant Archive (EMMA) - mouse sperm cryopreservation protocol [61].

Experimental design

C3-PMP22 study: Starting from post-natal day (PND) 15, mice were administered via oral gavage twice a day (bis in die (*b.i.d.*)). WT mice were administered with vehicle (saline solution: NaCl 0.9%) *b.i.d.* and C3-PMP22 mice were administered with vehicle *b.i.d.* or IFB-088 0.5mg/kg *b.i.d.* or 1mg/kg *b.i.d.* After 10-week treatment period, mice were tested for treadmill and grip-strength. After 12-week treatment period, mice were analysed for neurophysiology and sacrificed for morphology, and biochemistry. Each experiment was performed by a different operator, completely blinded to genotype and treatment.

***Mpz*R98C/+ study:** WT and *Mpz*R98C/+ mice were administrated via oral gavage twice a day with vehicle (saline solution: NaCl 0.9%) or IFB-088 1mg/kg starting from PND30. After 90 days (PND120) and 150 days (PND180) of treatment, mice were tested for rotarod, grip-strength and electrophysiology. Animals were then sacrificed for morphology, protein, and molecular expression analysis with the evaluator blinded to genotype and treatment.

Treadmill

C3-PMP22 mice were evaluated on treadmills after 10-week treatment. A grid that delivers a mild electric shock is used to motivate the animal to run. On the first day, mice are trained for 5mins, starting at 6cm/s; the speed is slowly increased to 10cm/s. The treadmill has a 5° inclination and delivers a 0.2mA shock. The following day, measurement is performed: initial speed is set up at 10cm/s, increased of 2cm/s every minute. The test ends at exhaustion, when the mouse spends more than three seconds on the electric shock grid. Distance covered, speed and number of shocks were recorded.

Rotarod

*Mpz*R98C/+ mice were evaluated at PND120 and PND180 on an accelerating rotating rod. Mice underwent three training trials on an IITC Life Science Roto-Rod (Series 8) with a ramp speed from 2 to 20rpm in 300s. A 1h rest was given after each trial and it was considered valid if the animals ran forward on the rod for at least 10s. The next day the latency to fall was recorded three times following the above-mentioned protocol for each time point and mouse. The average was used as the outcome value.

Grip strength

C3-PMP22 study

The muscular strength was evaluated using a GSM Grip-Strength Meter (Ugo basile). This test measures the muscular strength using an isometric dynamometer connected to a grid. Once the animal is holding the grid with its forepaws it is slowly moved backwards pulling the tail, until it

181 releases the grip. The dynamometer records the maximal force exerted. Each mouse is tested six
182 times.

183 ### *Mpz*R98C/+ study

184 The strength of all four limbs of WT and *Mpz*R98C/+ mice was evaluated using an automated
185 Grip Strength Meter (Columbus Instruments). Within 1 week after training (10 practice trials
186 using a mesh bar), the peak force exerted by each individual mouse was measured 10 times
187 consecutively with 10s resting periods and averaged.

188

189 ## Electrophysiological analysis

190 ### C3-PMP22 study

191 The electrophysiological evaluation was performed with a specific EMG system (NeuroMep
192 Micro, Neurosoft, Russia), as previously described [5]. Mice were anesthetized with
193 trichloroethanol, 0.02ml/g of body weight, and placed under a heating lamp to maintain constant
194 body temperature. Sciatic nerve conduction velocity was obtained by stimulating the nerve with
195 steel monopolar needle electrodes. A pair of stimulating electrodes was inserted subcutaneously
196 near the nerve at the ankle. A second pair of electrodes was placed at the sciatic notch to obtain
197 two distinct sites of stimulation, proximal and distal along the nerve. Compound motor action
198 potential (CMAP), was recorded with a pair of needle electrodes; the active electrode was
199 inserted in muscles in the middle of the paw, whereas the reference was placed in the skin
200 between the first and second digit. Sciatic nerve F-wave latency measurement was obtained by
201 stimulating the nerve at the ankle and recording the responses in the paw muscle, with the same
202 electrodes employed for the NCV study.

203 ### *Mpz*R98C/+ study

Mice were analyzed as above with the following differences. Anesthesia was with Ketamine/Xylazine (87.5mg/kg ketamine, 12.5mg/kg Xylazine). For sensory electrophysiological testing, one pair of loop electrodes were put 0.2cm and 0.7cm from the tail base as recording and reference electrodes. A second air was placed on the tail 3.7cm (cathode) and 4.2cm (anode) from the base. A ground electrode was put at the middle of two pairs loop electrodes. The distal pair was used for stimulation.

Morphological analysis

Mice were sacrificed at the indicated time points and sciatic and femoral nerves were dissected. Semi-thin section and electron microscope analyses were performed as previously described [14]. The number of amyelinated axons in C3-PMP22 mice was counted blind to genotype and treatment from quadricep femoral nerve semi-thin sections (0.5-1µm thick) stained with toluidine blue, on images taken with a 100x objective, after whole nerve reconstruction. Similarly, for *Mpz*R98C/+ mice, semithin sections were examined under a 63x objective. Each consecutive field was captured using a digital camera and whole nerve reconstruction was made by using photoshop software. In both studies, g-ratio analysis (axonal diameter/fiber diameter) and the size distribution of myelinated fibers (based on axons diameter) were also measured for all fibers. 4-8 mice per genotype and condition were analysed. Ultrathin sections (90nm thick) from femoral nerves were cut using an ultracut ultramicrotome, stained with uranyl acetate and lead citrate and examined by transmission electron microscopy (TEM) (Zeiss Leo912 Omega or JEOL 1230, Peabody, MA).

Protein extraction and Western Blotting

Mice were sacrificed at the indicated time points and sciatic nerves were dissected and immediately frozen in liquid nitrogen. Protein extraction was performed as previously described [52, 71]. The following antibodies were used: rabbit anti-Grp78/Bip (1:1000, Novus Biological, NB300-520 or 1:1000, Abcam, ab21685), rabbit anti-Phospho-eIF2α (Ser51) (D9G8) XP™ and eIF2α (D7D3) XP™ (1:2000, Cell Signalling, #3398 and #5324); chicken anti-P0 (PZO, Aves); rabbit anti-PMP22 (AB211052 or AB 861220; ABCAM); mouse anti-β-tubulin (1:1000, T4026, Sigma); mouse anti-Gapdh (1:1000, Millipore, MAB374); rabbit anti c-Jun (1:1000, ABCAM, #32137). Peroxidase-conjugated secondary antibodies (anti-rabbit HRP, DAKO, P0448; anti-chicken IgG-peroxidase, Sigma) were visualized using Amersham ECL or ECL Prime 225 reagent (GE Healthcare) for high-sensitivity chemiluminescent protein detection with UVItec gel analysis systems or using enhanced chemiluminescence (ECL) reagents (Bio-Rad) with autoradiography film (Kodak Scientific Imaging Film, Blue XB). Total proteins were visualized via staining with Coomassie Brilliant blue R250 staining solution (Bio-Rad). Densitometric quantification was performed with ImageJ.

RNA isolation and Real-time PCR analysis

C3-PMP22 study

Total RNA was extracted using TRIzol (Roche Diagnostic GmbH, Germany) and reverse transcription was performed as described previously [10] Quantitative RT-PCR was performed according to manufacturer's instructions (TaqMan, PE Applied Biosystems Instruments) on an ABI PRISM 7700 sequence detection system (Applied Biosystems Instruments). Normalization was performed using 18S rRNA as reference gene. Target and reference gene PCR amplification were performed in separate tubes with Assay on Demand™ (Applied Biosystems Instruments):

18S assay Hs99999901_s1; Ddit3/Chop, Mm00492097_m1; Xbp-1s assay, Mm03464496_m1; Hspa5/BiP assay, Mm00517691_m1; ATF4 assay, Mm00515324_m1; Gadd34/PPP1r15a assay, Mm00435119_m1.

*Mpz*R98C/+ study

Total RNA was extracted using NucleoSpin RNA Plus Kit (740984.50 Macherey-Nagel GmbH & Co. KG, Germany). Complementary DNA was prepared with SuperScript® III First Strand Synthesis SuperMix (11752-050, Invitrogen), and samples were analyzed as triplicates on a StepOnePlus Real-Time PCR System (Applied Biosystems) detection system using Fast SYBR® Green (4385612, Applied Biosystems). All samples were normalized to Ppia as an endogenous control and expressed relative (threshold cycle (Ct) and 2(-ΔΔCt)) to vehicle sciatic nerve data. The list of primers is below:

CHOP forward 5'-CTGCCTTTCACCTTGGAGAC-3'

CHOP Reverse 5'-CGTTTCCTGGGGATGAGATA-3'

BiP forward 5'-CATGGTTCTCACTAAAATGAAAGG-3'

BiP Reverse 5'-GCTGGTACAGTAACAACTG-3'

Xbp1-s forward 5'-GAGTCCGCAGCAGGTG-3'

Xbp1-s reverse 5'-GTGTCAGAGTCCATGGGA-3'

Ppia forward 5'-AGCACTGGAGAGAAAGGATT-3'

Ppia reverse 5'-ATTATGGCGTGTAAAGTCACCA-3'

IFB-088 pharmacokinetic study

Nine males and nine females C57BL/6J (three animals per sampling time) were treated with a single intraperitoneal administration of IFB-088 at 4 mg/kg. 10min, 30min, 1h, 2h, 4h, 6h, 8h

after administration, animals were briefly anaesthetized with Isofluorane and blood was collected. IFB-088 was extracted from plasma samples and measured by LC-MS/MS.

Statistical analysis

Group sizes were pre-determined with the G*Power v3.1.9.4 software (Heinrich-Heine-Universität Düsseldorf), to detect differences of at least 1,25 standard deviations between groups, with 80% power an alpha error of 0.05. Data were analysed with GraphPad Prism7.02 software. For behaviour and electrophysiology, outliers have been identified using Grubbs's test and data tested for normality and variance homogeneity. Statistical difference between mean values between two groups were tested using Student's T-test or Mann-Whitney. When multiple groups were compared, one-way ANOVA analysis followed by Friedman's, Tukey's or Dunnett's multiple comparison test and Kruskal-Wallis analysis followed by Dunn's multiple comparison test were used, as indicated in the Figure legends.

Results

*Mpz*R98C/+ DRG Schwann cell co-cultures show improved myelination following treatment with IFB-088

Explanted dorsal root ganglia (DRGs) from wild type (WT) and *Mpz*R98C/+ mice were plated and grown under myelinating conditions [12]. Similar to what was found in explants from *Mpz*Ser63del mice [12] the percentage of myelinated internodes was reduced in explant cultures of *Mpz*R98C/+ mice compared to explants from WT animals (Additional File 1: Supplementary Fig. 1 a-b), although higher than in *Mpz*S63del co-cultures. *Mpz*R98C/+ co-cultures were then

295 treated with escalating doses (50, 75, 100 and 125nM) of IFB-088 and assessed for myelination.
296 The number of myelinated internodes increased with all doses compared to untreated co-cultures
297 with a maximum effect at 100nM IFB-088 (Fig. 1a, Fig. 1b), similarly to what observed in
298 *Mpz*S63del explants (Additional File 1: Supplementary Fig. 1c-d and [12]).
299

300 IFB-088 treatment improves grip strength, rotarod performance and nerve 301 conduction velocities in *Mpz*R98C/+ mice

302 Western blot (WB) on sciatic nerve lysates from 1-month old *Mpz*R98C/+ mice, which
303 already manifested signs of the disease [56], showed a clear increase of P-eIF2α (Fig. 1c),
304 indicating activation of the PERK pathway of the UPR. We treated 1-month old WT and
305 *Mpz*R98C/+ mice with either vehicle or 1mg/kg of IFB-088 twice a day (the dosage shown to be
306 effective in *Mpz*S63del mice) [12] by oral gavage. Throughout the treatment mice were regularly
307 weighted. As previously reported for *Mpz*S63del mice [12], IFB-088 treatment does not impact
308 body weight (Additional File 1: Supplementary Fig. 2).

309 After 3- and 5-month of treatment mice were tested by Rotarod, Grip Strength, and by
310 neurophysiology. The mice were then sacrificed for morphological and biochemical analysis (Fig.
311 1d and Additional File 1: Supplementary Fig. 3a). As previously observed [12], IFB-088
312 treatment did not impact WT mice motor function or neurophysiological parameters (not shown).
313 *Mpz*R98C/+ mice had reduced grip strength compared to WT animals at PND120 (Additional
314 File 1: Supplementary Fig. 3b) and PND180 (Fig. 1e). After 5-month treatment *Mpz*R98C/+
315 mice showed significant improvement on grip strength compared to vehicle treated animals (Fig.
316 1e). Similar improvements were obtained for male and female mice (not shown). We evaluated
317 the mice on the same day for their ability to maintain balance on an accelerating Rotarod. We

confirmed a significant reduction in the latency to fall in PND120 and PND180 *Mpz*R98C/+ mice as compared to WT mice (Additional File 1: Supplementary Fig. 3c and Fig. 1f) [52, 56]. *Mpz*R98C/+ mice treated with IFB-088 for 5 months, but not 3 months, were able to maintain their balance significantly longer than untreated animals, approaching latencies obtained by WT animals (Fig. 1f and Additional File 1: Supplementary Fig. 3c).

Neurophysiological testing confirmed marked slowing in motor nerve conduction velocity (MNCV) and sensory nerve conduction velocity (SNCV) in *Mpz*R98C/+ mice at PND120 (Additional File 1: Supplementary Fig. 3d-e) and PND180 (Fig. 1g-h) [52, 56]. No significant differences in compound muscle action potential (CMAP) and sensory nerve action potential (SNAP) amplitudes were observed between WT and *Mpz*R98C/+ mice (not shown). 5-month treatment with IFB-088 significantly improved both MNCV and SNCV of *Mpz*R98C/+ mice (Fig. 1g-h). The positive impact of IFB-088 treatment on *Mpz*R98C/+ SNCV was also observed after 3-month of treatment (Additional File 1: Supplementary Fig. 3e).

IFB-088 treatment improves nerve morphology, partially reduces ER-stress and corrects the expression of Schwann cell differentiation marker in *Mpz*R98C/+ mice

On morphometric analysis, nerves from *Mpz*R98C/+ mice demonstrated marked abnormal myelin as attested by reduced myelin thickness and increased g-ratio (Fig. 2). After 5-month IFB-088 treatment, transverse sections of quadriceps femoral nerves from *Mpz*R98C/+ mice showed increased myelin thickness and reduced g-ratio (ratio between axon diameter and axon + myelin diameter) compared to vehicle treated nerves (Fig. 2a-e). Detailed ultrastructural

340 analysis performed via EM, confirmed the thin myelin sheath surrounding *Mpz*R98C/+ axons,
341 which appears thicker after IFB-088 treatment (Fig. 2f).

342 We previously showed that *Mpz*R98C/+ mice have increased expression of ER-
343 chaperones immunoglobulin heavy chain-binding protein (BiP) and glucose regulated protein 94
344 (Grp94), as part of an ER-stress response. We also demonstrated an altered phenotype of
345 myelinating Schwann cells in which the expression of c-Jun, a transcription factor that inhibits
346 myelination [50], was increased [56]. Therefore, we investigated the expression of mRNA (Fig.
347 3a-c), and protein levels (Fig. 3d-f) in a variety of genes known to play a role in these processes.
348 As previously described, *Mpz*R98C/+ mice presented an increase of the expression of ER-stress
349 and UPR markers *BiP*, C/EBP homologous protein (*Chop*) and spliced X-box-binding protein-1
350 (*Xbp1s*) and a higher level of c-Jun compared to WT mice (Fig. 3). IFB-088 treatment reduced
351 the levels of *Chop* and *BiP* mRNA and BiP protein, whereas the levels of *Xbp1s* were unchanged
352 (Fig. 3a-e). Finally, c-Jun protein levels were significantly reduced by IFB-088 (Fig. 3d, Fig. 3f).
353 Altogether our data suggest that treatment with IFB-088 reduced stress levels in *Mpz*R98C/+
354 nerves, allowing Schwann cell to differentiate and myelinate more efficiently.
355

356 **Nerves from the CMT1A mouse model C3-PMPP22 show alteration of myelin**
357 **proteins stoichiometry and activation of ER-stress pathways**

358 To address whether IFB-088 could be a viable treatment also for CMT1A we took
359 advantage of the C3-PMP22 mouse (supposed to carry 3-4 extra copies of PMP22) [65]. WB
360 performed of protein extract from C3-PMP22 nerves at 4-month demonstrated reduced
361 expression of P0 (MPZ), the most abundant myelin protein, but similar PMP22 levels to WT

nerves. As a result, there was a relative overexpression of PMP22 protein in C3-PMP22 nerves (Fig. 4a).

To test whether the excess of PMP22 would lead to proteostatic stress we measured the mRNA levels for a subset of well know UPR markers. This revealed a small increase in the expression of the general ER-stress marker *BiP* (downstream of the ATF6 arm of the UPR), and a significant upregulation of *Chop* and of the Protein Phosphatase 1 Regulatory Subunit 15A (*Gadd34/Ppp1r15a*), two downstream targets of the PERK/P-eIF2α pathway, whereas *Xbp1s*, a target of the inositol requiring enzyme 1 (IRE1) arm, and the activating transcription factor 4 (*Atf4*) were not increased (Fig. 4b). WB for BiP and P-eIF2α confirmed the activation of stress pathways in these nerves (Fig. 4c-d). These results showed that C3-PMP22 mice present an alteration of myelin proteins stoichiometry associated with the activation of ER-stress pathways.

IFB-088 treatment improves motor capacity and MNCV in CMT1A mice

We treated C3-PMP22 mice with either 0.5mg/kg or with 1mg/kg of IFB-088 twice a day by oral gavage. The treatment started at PND15, when the disease is already manifested as shown by severe myelination defects, altered myelin proteins stoichiometry and activation of ER-stress pathways (Additional File 1: Supplementary Fig. 4).

After 10-week of treatment C3-PMP22 mice were tested for motor capacity and, after 12-week of treatment, for neurophysiology. They were then sacrificed for morphological and biochemical analysis (Fig. 5a). Treadmill analysis showed that C3-PMP22 mice were severely impaired compared to WT mice (Fig. 5b). IFB-088 treatment at 1mg/kg *b.i.d.* showed a small but significant improvement as compared to vehicle treated mice (Fig. 5b). However, the operator (blind to treatment) noticed that all C3-PMP22 male mice ran very poorly. Therefore, the mice

were stratified by gender. C3-PMP22 female mice treated with IFB-088 1mg/kg *b.i.d.* had a significant amelioration in motor capacity, that increased 2-fold compared to vehicle treated mice (Fig. 5c). Male mice also had a comparable 2-fold improvement with the same dosage, but the baseline was very poor (Fig. 5d).

Grip strength confirmed that C3-PMP22 mice were impaired compared to WT mice. IFB-088 treatment did not improve strength when the mice were analysed altogether (Fig. 5e). However, when divided by gender, C3-PMP22 male mice showed a trend towards improvement at 0.5mg/kg *b.i.d.* which became significant for the 1mg/kg *b.i.d.* of IFB-088 (Fig. 5g). This positive impact was not seen in C3-PMP22 female mice (Fig. 5f).

Finally, we assessed a series of neurophysiological parameters (MNCV, F-wave latency, CMAP) which revealed a severe impairment in C3-PMP22 mice as compared to WT controls (Fig. 5h and not shown), as previously reported [65]. Treatment with both 0.5 and 1mg/kg *b.i.d.* IFB-088 showed a modest improvement in MNCV after 12-week treatment, that reached significance for the 0.5mg/kg *b.i.d.* dose (Fig. 5h). Stratification per gender revealed that the improvement was restricted to female mice, for which the amelioration was statistically significant at both dosages (Fig. 5i). Only IFB-088 treated C3-PMP22 female mice displayed MNCV over 20m/s. On the contrary in C3-PMP22 male mice there was no improvement, and actually the 1mg/kg *b.i.d.* dose showed a small worsening that, although marginal, reached statistical significance (Fig. 5j). None of the other neurophysiological parameters measured were improved by the treatment (not shown).

IFB-088 treatment improves nerve morphology, reduces ER-stress level and partially readjust myelin proteins stoichiometry in CMT1A mice

Previous analysis suggested that C3-PMP22 mice motor nerves were more affected than sensory nerves [24, 65]. Therefore, we dissected quadriceps femoral nerve, predominantly motor, and sciatic nerve which is a mixed nerve with many sensory axons. Transverse sections of sciatic nerves showed an increase in the myelination of large calibre fibres in mice treated with IFB-088. In both male and female C3-PMP22 nerves large calibre axons were almost invariably amyelinated (where by amyelinated we refer to any axon with diameter>1µM, which is in contact with a Schwann cell but not myelinated by it). After IFB-088 treatment many of the large axons were myelinated (Additional File 1: Supplementary Fig. 5). Similarly, in untreated femoral nerves most large calibre axons were amyelinated whereas small calibre axons tended to be hypermyelinated (Fig. 6a-b). As in sciatic nerves, treatment with IFB-088 partially corrected these abnormalities with myelin wrapping appearing around large axons at both 0.5 and 1mg/kg *b.i.d.* of IFB-088 (Fig. 6a-b). No gross differences were detected between female and male nerves (Additional File 1: Supplementary Fig. 5 and Fig. 6a-b).

Cross sections of the entire femoral nerve from 2-4 mice per condition for both genders were reconstructed and, for each nerve, the entire number of myelinated or amyelinated axons was counted (Table 1).

Table 1 Percentage of amyelinated (amongst axons with diameter larger than 1 µm) and myelinated fibres. Data were expressed in percentage of fibers as mean ± SEM. *n*=5-8 mice per condition. **P*<0.05, ***P*<0.01 by One-way ANOVA with Tukey post-hoc test; §*P*<0.05 by Student's T-test vs C3-PMP22 vehicle.

		WT Vehicle *b.i.d.*	C3 Vehicle *b.i.d.*	C3 IFB-088 0.5 mg/kg *b.i.d.*	C3 IFB-088 1 mg/kg *b.i.d.*
% of amyelinated fibers	All mice	0.033 ± 0.08	27.2 ± 2.4	**19.9 ± 1.3****	21.9 ± 1.4
	Females	0.1 ± 0.06	29.9 ± 1	19.8 ± 2.5§	23.5 ± 0.3
	Males	0	25.4 ± 3.9	20 ± 1.2	20.3 ± 2.7
% of myelinated fibers	All mice	100 ± 0.026	72.8 ± 2.4	**80 ± 1.3***	78.1 ± 1.4
	Females	99.8 ± 0.061	70.1 ± 1	80.1 ± 2.5§	76.5 ± 0.3
	Males	100	74.6 ± 3.9	80 ± 1.2	79.7 ± 2.7

This analysis identified 27.2 ± 2.4% amyelinated large axons in C3-PMP22 vehicle treated nerves. Treatment with IFB-088 0.5 or 1mg/kg *b.i.d.* reduced the percentages to 19.9±1.3% and 21.9±1.4%, representing a 27% and 20% improvement respectively. The number of amyelinated axons was slightly greater for females (29.9±1%) than for males (25.4±3.9%) which also showed more variability. In males the treatment with IFB-088 0.5 or 1mg/kg *b.i.d.* had a similar effect, reducing amyelinated axons by roughly 20%, whereas in females the IFB-088 0.5mg/kg *b.i.d.* treatment reduced amyelinated axons by 34%, while the IFB-088 1mg/kg *b.i.d.* treatment reduced it by 20% (Table1).

Analysis of myelin thickness by g-ratio showed a remarkable difference in the scatter plot between WT and C3-PMP22 mice. The slope for C3-PMP22 mice was much steeper, mostly due to the large group of hypermyelinated small axons (diameter < 1 μM) accompanied by the almost complete absence of myelination in axons larger than 5μM (Fig. 6c). Indeed, whereas there were no myelinated axons smaller than 1μM in WT nerves, 4.4% of the axons myelinated in quadriceps femoral nerves from C3-PMP22 mice had a diameter lower than 1μM, indicating an aberrant hypermyelinating phenotype. Conversely, 45.9% of myelinated axons in nerves from WT mice had a diameter larger than 5μM, a percentage that was reduced to only 3.9% of the myelinated axons in C3-PMP22 mice (Fig. 6d). IFB-088 treatment partially corrected these abnormalities. The percentage of myelinated axons smaller than 1μM was reduced to 2.1% and 2.3% by the IFB-088 0.5mg/kg *b.i.d.* and 1mg/kg *b.i.d.* treatment respectively, whereas the percentage of myelinated axons with a diameter larger than 5μM rose to 12.4% and 8.5% respectively (Fig. 6d). Stratification of male and female mice showed that the amelioration in the hypermyelinating phenotype in small calibre axons was exclusively present in females, as visible

in the scatterplots (Additional File 1: Supplementary Fig. 6a-b), even though the overall g-ratio in vehicle treated C3-PMP22 males and females was virtually identical (0.61±0.013 in males vs 0.61±0.015 in females). In both C3-PMP22 males and females, IFB-088 treatment increases the number of myelinated axons with diameter larger than 5μM (Additional File 1: Supplementary Fig. 6c-d).

Detailed analysis by transmission electron microscopy (TEM) on transverse sections from quadriceps femoral nerves confirmed that in C3-PMP22 nerves, small diameter axons (even smaller than 1μm) were surrounded by an abnormally thick myelin sheath. In female nerves, treatment with IFB-088 almost completely corrected this phenotype (Fig. 6e and Additional File 1: Supplementary Fig. 6a). At the same time, large calibre axons were either not myelinated or presented a very thin layer of myelin (probably corresponding to 2-3 wraps of Schwann cell membrane). Treatment with IFB-088 allowed myelination to proceed also in large calibre fibres (Fig. 6f). Importantly, this newly formed myelin appeared to have a proper structure and compaction/periodicity.

As previously shown, C3-PMP22 nerves presented increase expression of the ER-stress marker BiP and an unbalance between PMP22 and P0 protein levels. We therefore wanted to test whether IFB-088 treatment could correct these features. WB analysis showed that treatment with both dosages of IFB-088 normalized BiP expression to WT levels (Fig. 7a-b), and that there was a partial (although not complete) readjustment of the PMP22/P0 protein ratio (Fig. 7a, Fig. 7c), suggesting an overall improvement in nerve proteostasis.

Discussion

The maintenance of correct protein homeostasis (proteostasis) is tightly controlled by protein quality control (PQC) mechanisms [1]. Myelinating Schwann cells, that need to synthesize large amounts of lipids and proteins, are particularly susceptible to failures in PQC. Alterations in proteostasis, deficits in PQC and the activation of ER-stress/UPR have been implicated in several myelin disorders [69]. Here we show that the small molecule IFB-088 is able to readjust protein homeostasis and to ameliorate disease features in two models of demyelinating CMT1, the *Mpz*R98C/+ (CMT1B) and the C3-PMP22 (CMT1A) mice.

IFB-088 improves disease features in CMT1B mice

We demonstrated that IFB-088 effectively mitigates the peripheral neuropathy in *Mpz*R98C/+ mice, using *in vitro* as well as *in vivo* studies. *In vitro*, IFB-088 enhanced myelination in *Mpz*R98C/+ DRGs explant co-cultures. *In vivo*, 5-month IFB-088 treatment improved motor performance, nerve conduction velocity, and peripheral nerve morphology of *Mpz*R98C/+ mice. Our prior studies demonstrated that ER-chaperones such as BiP and the transcription factor CHOP are upregulated in *Mpz*R98C/+ mice consistent with their ER-stress response. We also previously demonstrated that the transcription factor c-Jun, which inhibits PNS myelination [50], was upregulated in *Mpz*R98C/+ mice [56]. We now show that treatment with IFB-088 reduced ER-stress and decreased the expression of the negative regulator of myelination c-Jun.

IFB-088 treatment effects, while significant in *Mpz*R98C/+ mice, were less pronounced than those observed in *Mpz*Ser63del animals [12]. Morphological as well as molecular deficits were often prevented in the *Mpz*Ser63del mice [12] but only showed improvement in the *Mpz*R98C/+. We posit several reasons for these differences. First, *Mpz*R98C/+ mice may be considered a “more authentic disease model” than the *Mpz*Ser63del animals, and this may

497 contribute to the different responses to treatment between the two models. The *Mpz*R98C/+ mice
498 have had the mutation "knocked in" to the endogenous mouse *Mpz* allele [56]. Alternatively, the
499 *Mpz*Ser63del mice are transgenic animals and still retain two WT *Mpz* alleles in addition to the
500 *Mpz*Ser63del expressing transgene [70]. Thus, *Mpz*Ser63del mice have two copies of WT *Mpz* as
501 opposed to the one *Mpz*R98C/+ mice to generate the normal protein. Secondly, the R98C *MPZ*
502 neuropathy in humans is more severe than that caused by Ser63del *MPZ*. Patients with R98C
503 *MPZ* (also called R69C by an earlier numbering system) have a dysmyelinating neuropathy and
504 present with delayed developmental milestones, often not walking independently until after 2
505 years of age. Affected patients may require walkers or wheelchairs for ambulation prior to
506 reaching adulthood, and typically have MNCV<10 m/s [3, 55]. Patients with the Ser63del *MPZ*
507 mutation typically reach developmental milestones on time, walk independently by a year of age
508 and only slowly develop symptoms over the first two decades of life. They have not required
509 more than ankle foot orthotics to ambulate even in adulthood [41]. In humans *MPZ*S63del
510 MNCV are in the 20-30m/s range, similar to what is observed in patients with CMT1A [41].
511 Thus, clinically, the Ser63del *MPZ* mutation is considered to be a demyelinating rather than a
512 dysmyelinating neuropathy. Taken together these data suggest the *Mpz*R98C mouse model
513 causes a more severe neuropathy, that would be expected to be more difficult to reverse than the
514 neuropathy caused by the Ser63del *Mpz* mutation.

515 How alleviating ER-stress improves the neuropathy caused by the R98C and Ser63del
516 *MPZ* mutations remains an important issue. It is unlikely that augmenting UPR activity improves
517 myelination by allowing R98C P0 to be transported to and inserted into PNS myelin. Introducing
518 a cysteine into the P0 extracellular domain at codon 98 would be predicted to disrupt the di-
519 sulfide bridge between existing cysteines at codons 50 and 127 [59]. This would in turn disrupt

the secondary and tertiary structures of the extracellular domain that are necessary to create P0 tetramers in cis and trans to compact myelin [59], as already elegantly shown for the *Mpz*S63C mutation [2, 70]. We believe it more likely that treatment benefits from IFB-088 occur by facilitating the Schwann cells ability to degrade the R98C P0 as well as transport WT P0 to myelin. Myelinating Schwann cells generate very large amounts of proteins and lipids to form and maintain the myelin sheath [42, 44]. Processing and properly folding P0 glycoprotein in the ER is particularly demanding as P0 is, by far, the major PNS myelin protein, comprising approximately 50% of all PNS myelin proteins [22] and 2% of all Schwann cell transcripts during the peak of myelination [36]. Folding and post-translationally processing P0 by ERQC pathways is a major undertaking for the ER, even when the protein is in its WT form [13]. The task is increased when a mutation such as R98C makes folding the protein more difficult. Schwann cells typically target misfolded proteins for degradation, through ubiquitination and proteasomal processing. Both protein degradation and proteosome function have been shown to be impaired in *Mpz*Ser63del mice [67, 68] and this is likely to be the case with *Mpz*R98C/+ mice as well. We predict that IFB-088-mediated translational attenuation through persistent phosphorylation of eIF2α, will better enable Schwann cells to target R98C P0 to the proteosome, readjusting protein homeostasis as shown in *Mpz*Ser63del mice [11, 12]. In support of this hypothesis, it has been recently shown that promoting degradation by stimulating the proteasome ameliorates proteostasis and improves the phenotype of *Mpz*Ser63del mice [66]. We have previously shown that UPR activation causes *Mpz*R98C and *Mpz*S63del Schwann cells to enter a limited differentiation state in part by upregulating c-Jun expression; c-Jun, a transcription factor, negatively regulates myelination [50] [16]. As a result of this inhibition, myelin protein expression, including P0, decreases so that there is less mutant P0 for the ER to process [56].

IFB-088 treatment reduces the expression of the UPR marker BiP in *Mpz*R98C/+ mice, suggesting a reduction of ER-stress upon treatment. In addition, IFB-088 treatment decreases c-Jun expression and increases peripheral nerve myelination suggesting that inhibition of myelination is lifted. Restoring the Schwann cell phenotype will enable more WT P0 from the normal allele to reach myelin and contribute to clinical improvement. Supporting this explanation is the fact that we have recently demonstrated that patients who are haploinsufficient of *MPZ* have only a mild, late onset neuropathy, much milder than the neuropathy caused by R98C or Ser63del *MPZ* mutations [28].

C3-PMP22 mice show altered proteostasis

The overexpression of PMP22 in animal models is sufficient to cause neuropathy, suggesting that increased dosage of PMP22 is the main contributing factor in CMT1A pathology [29, 58]. How the extra copy of *PMP22* causes disease is not fully understood, but studies in rodent models as well as in CMT1A patient derived fibroblast show that PMP22 can form cytosolic aggregates accompanied by reduced proteasomal activity, which may ultimately lead to cytotoxicity [17, 35, 45], PMP22 is a highly metastable protein, with more than 80% of newly synthesized PMP22 rapidly degraded by the proteasome, via ER-associated degradation (ERAD) [48, 49]. Recent *in vitro* work suggested that in normal condition, the levels of expression of PMP22 are close to the saturation capacity of the ERQC systems, and that overexpression of PMP22 leads to a disproportionate increase in misfolding and mis-trafficking [40]. Accordingly, examination of sciatic nerve from C22 mice, which show a severe dysmyelinating neuropathy, revealed increased expression of UPR markers such as BiP and CHOP [23]. In human, levels of PMP22 protein in CMT1A patient skin biopsies are elevated, even though the levels are more

566 variable than in non-CMT1A samples [31, 37]. High levels of PMP22 protein have also been
567 reported in sural nerve biopsies from CMT1A patients [19, 64]. Although the exact mechanism
568 underlying the pathogenicity associated with expression of third copy of *PMP22* is not yet
569 clearly defined, it is well established that a correct stoichiometry of PMP22 protein is required to
570 maintain compact myelin integrity [27, 30]. Correction of PMP22 expression level reverses
571 demyelination phenotype in a transgenic animal model [54] and the relevance of reducing
572 PMP22 expression has been acknowledged as one potential therapeutic approach for CMT1A
573 [47]. Recently, several approaches aimed at reducing PMP22 mRNA expression, such as anti-
574 sense oligonucleotides (ASO), siRNA and AAV2/9-mediated shRNA targeting PMP22 have
575 been successfully tested in murine models [6, 7, 20, 73], but their translation to humans still
576 poses several hurdles.

577 We reasoned that a pharmacologic approach like IFB-088 aimed at attenuating general
578 protein translation, thus reducing also PMP22 levels, would currently represent a more viable
579 option than gene therapies. For this study we used the C3-PMP22 mice, that carry 3-4 copies of
580 the human *PMP22* gene, and that is thought to represent the more appropriate model to study
581 CMT1A, as compared to C22 mice (carrying 7-8 copies) [65]. We showed that in C3-PMP22
582 mice PMP22 overexpression results in the activation of the stress sensor BiP and of the PERK/P-
583 eIF2α pathway of the UPR, which supports the idea that activation of a stress response could be
584 a contributing factor in CMT1A pathogenesis.

585

586 **IFB-088 treatment improves disease features in CMT1A mice**

587 Treatment with IFB-088 improved motor capacity, neurophysiology, peripheral nerve
588 morphology, and partially readjusted both myelin protein stoichiometry and stress levels in C3-

PMP22 CMT1A mice. Importantly the treatment was started at PND15, when morphological deficits are already evident and ER-stress already activated, indicating that the treatment is ameliorating the disease and not simply preventing it. Intriguingly, some of these improvements were more prominent (treadmill) or present exclusively (neurophysiology) in females, whereas the improvement in dysmyelination was detectable in both sex although, again, some morphological parameters were ameliorated more in females than in males. The reasons for these differences are not clear. We ruled out a difference in IFB-088 exposure in males and females, as, in C57BL/6J mice, the same background as the C3-PMP22, no difference in term of IFB-088 pharmacokinetic profile was observed (Additional File 1: Supplementary Fig. 7). Moreover, we did not detect significant gender differences in the response to treatment in *Mpz*R98C/+ mice (this study), nor in *Mpz*S63del mice [12]. These results suggest that the difference may be more specific to the C3-PMP22 model itself. Of note, differences in motor capacity between genders have already been observed in different experimental setting in C3-PMP22 mice (F. Baas, *unpublished*) and in rotarod in the C22 model, with males performing significantly worse than females [51].

Neurophysiology analysis revealed an amelioration in nerve conduction velocity exclusively in females. The strong neurophysiological impairment in C3-PMP22 mice was accompanied by a complex and severe dysmyelinating phenotype, characterized by hypermyelination of small fibers and almost complete amyelination of large fibers, consistent with previous reports [65]. While myelination of large fibers improved almost equally in males and females after treatment with IFB-088, small fibers hypermyelination was more efficiently corrected in females. Whether this difference in morphological rescue is sufficient to explain the

611 discrepancy in NCV after treatment remains unclear however as the speed of NCV depends
612 predominantly on large diameter fibers [34].

613 The dysmyelinating phenotype in C3-PMP22 mice was accompanied by an increase in
614 the levels of the ER-stress marker BiP and of P-eIF2α. Conversely, *Xbp1s* levels did not change
615 significantly between WT and C3-PMP22 nerves, indicating that, unlike the CMT1B models
616 *Mpz*R98C/+ and *Mpz*S63del, not all the UPR pathways were activated by PMP22 overexpression.
617 This difference is likely related to different mechanisms of stress activation in the two models:
618 whereas R98C and Ser63del P0 are misfolded proteins retained in the ER [53, 56, 70] where they
619 activate a canonical UPR, overexpression of PMP22 is thought to overwhelm the ERAD-
620 proteasome system, and the activation of ER-stress is likely a secondary event. In this respect it
621 has been shown that ERAD impairment in Schwann cells results in ER-stress activation [68, 72].
622 We hypothesize that by prolonging the phosphorylation of eIF2α, IFB-088 attenuates the
623 translational of highly expressed myelin proteins including PMP22. As a result, stress levels
624 were restored towards WT levels in treated C3-PMP22 mice, and there was a partial
625 readjustment of protein stoichiometry in nerves from both male and female mice.

626 Despite these very promising results, the C3-PMP22 was only partially improved, and not
627 fully rescued, probably because, as for *MPZ*R98C/+ mice, the dysmyelinating phenotype of these
628 mice is very severe to start with. Several questions remain to be answered, including whether a
629 prolonged treatment beyond 4-month of age would further improve the phenotype, and whether a
630 treatment initiated in adult mice would still provide benefits. Moreover, it should be noted that
631 while the C3-PMP22 mouse represents a good model of CMT1A, currently there is no authentic
632 animal model for this disease, as all available models express extra copies of the *PMP22* gene
633 but without replicating the 1.4Mb duplication found in humans.

In summary, we have demonstrated that IFB-088 treatment improved the neuropathy in *Mpz*R98C/+ mice, a CMT1B mouse model, and in C3-PMP22 mice, a CMT1A mouse model. This is the second example of IFB-088's ability to improve the neuropathy in a mouse model of CMT1B. We have identified many additional mutations in *MPZ* that activate the UPR [4] and expect that IFB-088 may prove beneficial in many of these patients. In addition, our study confirms a role of ER-stress in the pathogenesis of CMT1A and demonstrate the ability of IFB-088 to assist the ER-stress response to the over-expression of PMP22 and potentially treat patients with CMT1A. Thus, IFB-088, which completed successfully phase I clinical trial, represents a new and promising therapeutic option for CMT1A and CMT1B. Due to his mode of action, IFB-088 has the unique potential to provide benefits to different CMT subtypes caused by different gene defects. Moreover, the benefits of IFB-088 have been also demonstrated in Amyotrophic Lateral Sclerosis and in Multiple Sclerosis models [8, 9, 12], suggesting that managing UPR and ER-stress are promising strategies for multiple neurodegenerative diseases.

Abbreviations: AD = autosomal dominant; AR = autosomal recessive; ASO = anti-sense oligonucleotides; ATF4 = activating transcription factor 4; BiP = immunoglobulin heavy chain-binding protein; CHOP = C/EBP homologous protein; CMT = Charcot Marie Tooth; CMAP = compound muscle action potential; DRG = dorsal root ganglia; eIF2α = alpha subunit of the eukaryotic translation initiation factor 2; ER = endoplasmic reticulum; ERAD = ER-associated degradation; ERQC = endoplasmic reticulum protein quality control; Grp94 = glucose regulated protein 94; IRE1 = inositol requiring enzyme 1; MBP = myelin binding protein; MPZ = myelin protein zero; MNCV = motor nerve conduction velocity; NCV = nerve conduction velocity; NF = neurofilament; PERK = protein-kinase RNA-like endoplasmic reticulum kinase; PMP22 =

peripheral myelin protein 22; PND = post-natal day; PPP1R15A = Protein Phosphatase 1 Regulatory Subunit 15A; PQC = protein quality control; SNAP = sensory nerve action potential; SNCV = sensory nerve conduction velocity; UPR = unfolded protein response; Tr^{J} = Trembler J; TEM = transmission electron microscopy; WB = western blot; WT= wild type; XBP1 = X-box-binding protein-1.

Declarations

Availability of data and materials

The data that support the findings of this study are available from the corresponding author, upon reasonable request.

Competing interests

P.G., P.M. and C.T. are full-time employees and stockholders of InFlectis BioScience. M.D. acts as a Scientific Advisory Board member for InFlectis BioScience.

Funding

This work was funded by InFlectis BioScience.

Authors' contributions

M.D., M.E.S., P.G., P.M., C.T. contributed to the study conception and design. F.B. provided the C3-PMP22 mouse model. R.M. performed the myelinating DRG explant cultures. Y.B. and DW

679 performed the study in the MpzR98C/+ mouse model. V.G.V., C.S., C.F., R.M., T.T., F.F.,
680 performed the study in the C3-PMP22 mouse model. F.B., U.D. performed the
681 neurophysiological evaluation of the C3-PMP22 mice. M.D., M.E.S. and C.T. wrote the
682 manuscript. All authors commented on previous versions of the manuscript. All authors read and
683 approved the final manuscript.

684

685 Acknowledgements

686 We thank the Charcot-Marie-Tooth Association for their continuous support. We are grateful to
687 Dr. Patrizia D'Adamo and the Mouse Behavior Facility at IRCCS Ospedale San Raffaele. Part of
688 this work was carried out in ALEMBIC, an advanced microscopy laboratory established by
689 IRCCS Ospedale San Raffaele and Università Vita-Salute San Raffaele. M.D. is supported by
690 Fondazione Telethon (GGP19099), CMTA (Charcot-Marie-Tooth Association, USA) and
691 CMTRF (Charcot-Marie-Tooth Research Foundation).

692

693 **Additional file 1:** Supplementary figures S1 - S7.

694

695

696 Figure legends

697

698 **Figure 1: IFB-088 improves myelination in DRG explants, motor function and nerve**
699 **conduction velocity from *Mpz*R98C/+ mice.** Dorsal root ganglia (DRG) were dissected from
700 embryos (E13.5) of *Mpz*R98C/+ mice. The myelination process was induced with ascorbic acid.

After 2-week of treatment with vehicle or the indicated concentration of IFB-088, the DRGs were fixed and nuclei visualized by DAPI staining; axons and myelin were visualized by immunostaining with neurofilament antibody (NF) and with myelin basic protein (MBP) antibodies respectively. (**a**) Representative pictures. (**b**) Number of myelinated internodes per field in *Mpz*R98C/+ DRG explant cultures treated with vehicle or the indicated concentration of IFB-088 for 2 weeks. Mean ±SEM. *n*=3 independent experiments. **P*<0.05 One-way ANOVA followed by Friedman's test. (**c**) Representative western blot (WB) for P-eIF2α and tubulin on sciatic nerve protein extracts from 1-month-old WT and *Mpz*R98C/+ mice. (**d**) Diagram of the treatment strategy. 30-day-old WT and *Mpz*R98C/+ mice were orally administered with vehicle or IFB-088 1mg/kg *b.i.d.* for 5-month. (**e**) Four limb grip strength max values average of 10 trials. Data were expressed in grams (g) as mean ±SEM. *n*=15-26 mice per condition. (**f**) Rotarod analysis. Data are expressed in seconds (s) as mean ±SEM. *n*=15-26 mice per condition. (**g**) Motor nerve conduction velocity (MNCV). Data are expressed in meter/second (m/s) as mean ±SEM. *n*=15-27 mice per condition. (**h**) Sensory nerve conduction velocity (SNCV). Data are expressed in meter/second (m/s) as mean ±SEM. *n*=15-26 mice per condition. ***P*<0.01; ****P*<0.001, *****P*<0.0001 by Student's T-test; ###*P*<0.001, ####*P*<0.0001 by Mann-Whitney.

Figure 2: IFB-088 treatment improves *Mpz*R98C/+ mice quadriceps femoral nerve morphology. (a) Toluidine blue stained semithin sections of quadriceps femoral nerve from *Mpz*R98C/+ mice treated with vehicle *b.i.d.* or IFB-088 1mg/kg *b.i.d.* for 5 months. Arrows illustrate myelinated axons. Scale bar, 20µm. (**b**) Quadriceps femoral nerve g-ratios from *Mpz*R98C/+ mice treated with vehicle *b.i.d.* or IFB-088 1mg/kg *b.i.d.* for 5 months. Data are

724 expressed as mean ±SEM. *n*=4 mice per condition. **P*<0.05 by Student's T-test. (**c**) Scatter plot
725 of quadriceps femoral nerve g-ratios toward axon diameter from *Mpz*R98C/+ mice treated with
726 vehicle *b.i.d.* or IFB-088 1mg/kg *b.i.d.* *n*=4 mice per condition. (**d**) Myelin thickness of
727 quadriceps femoral nerve from *Mpz*R98C/+ mice treated with vehicle *b.i.d.* or IFB-088 1mg/kg
728 *b.i.d.* for 5 months. Data are expressed in µm as mean ±SEM. *n*=4 mice per condition. **P*<0.05
729 by Student's T-test. (**e**) Scatter plot of quadriceps femoral nerve myelin thickness toward axon
730 diameter from *Mpz*R98C/+ mice treated with vehicle *b.i.d.* or IFB-088 1mg/kg *b.i.d.* *n*=4 mice
731 per condition. (**f**) Ultrathin sections of quadriceps femoral nerve from WT mice treated with
732 vehicle *b.i.d.* and from *Mpz*R98C/+ mice treated with vehicle *b.i.d.* or IFB-088 1mg/kg *b.i.d.* for
733 5 months. Lower panels are higher magnification images of upper panels. Scale bar 1µm for top
734 panels, and 500nm for bottom panels.
735
736 **Figure 3: IFB-088 treatment reduces ER stress and Schwann cells differentiation markers**
737 **expression in *Mpz*R98C/+ sciatic nerve.** Evaluation of mRNA (**a-c**) and protein levels (**d-f**) on
738 sciatic nerve samples from WT and *Mpz*R98C/+ mice treated with vehicle *b.i.d.* or IFB-088
739 1mg/kg *b.i.d.* for 5 months. mRNA relative levels of *Bip* (**a**), *Chop* (**b**) and *Xbp1s* (**c**) determined
740 by qRT-PCR. *n*=4 per condition. #*P*<0.05 by Mann-Whitney. (**d**) Western blot images for BiP
741 and c-Jun. Quantification relative to tubulin for BiP (**e**), and c-Jun (**f**). *n*=2-5 per condition.
742 **P*<0.05, ***P*<0.01 by Student's T-test.
743
744 **Figure 4: C3-PMP22 mice show a relative overexpression of PMP22 associated with**
745 **expression of ER stress/UPR markers.** (**a**) Evaluation of PMP22, P0 and GAPDH protein
746 levels by WB in sciatic nerve protein lysates from 4-month-old WT and C3-PMP22 (C3) mice.

Top: Representative picture. Bottom: Quantification of the PMP22/P0 protein ratio. *n*=3 per condition. **P*<0.05 by Student's T-test. (**b**) Evaluation of *Bip*, *Chop*, *Xbp1s*, *Atf4* and *Gadd34/Ppp1r15a* mRNA levels by qRT-PCR on sciatic nerve samples from 4-month-old WT and C3-PMP22 (C3) mice. *n*=4 per condition. #*P*<0.05 Mann Whitney. (**c**) Evaluation of BiP and tubulin protein levels by WB in sciatic nerve protein lysates from 4-month-old WT and C3-PMP22 (C3) mice. Top: Representative picture. Bottom: Quantification relative to tubulin. *n*=6 per condition. Student's T-test. (**d**) Evaluation of eIF2α phosphorylation level and tubulin protein level by WB in sciatic nerve protein lysates from 1-month-old WT and C3-PMP22 (C3) mice. Top: Representative picture. Bottom: quantification of eiF2α phosphorylation level relative to tubulin. *n*=6 per condition. Student's T-test.

Figure 5: IFB-088 treatment improves motor function and nerve conduction velocity in C3-PMP22 mice. (**a**) Diagram of the treatment strategy. 15-day-old WT and C3-PMP22 (C3) mice were orally administered with vehicle *b.i.d.* or IFB-088 at 0.5 or 1mg/kg *b.i.d.* for 12 weeks. (**b**) Treadmill analysis performed after 10-week of treatment. Data from males and females expressed in meter (m) as mean ± SEM. *n*=14-22 mice per condition. (**c**) Data from females. *n*=8-10 mice per condition. (**d**) Data from males. *n*=6-13 mice per condition. (**e**) Forepaws grip strength average of 6 trials performed after 10-week of treatment. Data were expressed in pull force (grams) as mean ± SEM. *n*=14-22 mice per condition. (**f**) Data from females. *n*=8-10 mice per condition. (**g**) Data from males. *n*=6-13 mice per condition. (**h**) Motor nerve conduction velocity (MNCV) performed after 12-week of treatment. Data from males and females expressed in meter/second (m/s) as mean ±SEM. n=14-21 mice per condition. (**i**) Data from females. *n*=8-10 mice per condition. (**j**) Data from males. *n*=6-12 mice per condition. **P*<0.05; ***P*<0.01;

770 ****P<0.0001 by Student's T-test. #P<0.05; ###P<0.001; ####P<0.0001 by Mann-Whitney.
771 &P<0.05; &&P<0.01 by One-Way ANOVA followed by Dunnett's test. $$P$<0.05; $$$P$<0.01;
772 $$$$P$<0.001 by Kruskal-Wallis followed by Dunn's test.
773
774 **Figure 6: IFB-088 treatment improves C3-PMP22 mice quadriceps femoral nerve**
775 **morphology.** Toluidine blue stained semithin sections of quadriceps femoral nerve from (**a**)
776 female and (**b**) male WT mice treated with vehicle *b.i.d.* and C3-PMP22 (C3) mice treated with
777 vehicle *b.i.d.* or IFB-088 at 0.5 or 1mg/kg *b.i.d.* for 12 weeks. Scale bar, 10µm. (**c**) Scatter plot
778 of quadriceps femoral nerve g-ratios from WT mice treated with vehicle *b.i.d.* and C3-PMP22
779 (C3) mice treated with vehicle *b.i.d.* or IFB-088 at 0.5 or 1mg/kg *b.i.d*. Note the "cloud" of axons
780 with diameter lower than 1µm present only in C3-PMP22 nerves (untreated and treated) and the
781 appearance of a considerable number of myelinated axons larger than 5-6µm in IFB-088 treated
782 C3-PMP22 nerves. *n*=5-8 nerves per condition. (**d**) Percentage of myelinated axons per axons
783 size. *n*=5-8 nerves per condition. (**e** and **f**) TEM analysis of quadriceps femoral nerve from C3-
784 PMP22 (C3) mice treated with vehicle *b.i.d*. or IFB-088 at 1mg/kg *b.i.d*. (**e**) In C3-PMP22
785 vehicle treated nerves, small calibre axons are abnormally hypermyelinated (black dotted arrows).
786 Treatment with IFB-088 results in normal looking myelin in axons larger than 1µm (red arrows)
787 or in almost no myelin is smaller axons (blue larges arrows). (**f**) In C3-PMP22 vehicle treated
788 nerves large calibre axons are basically amyelinated or with only a very thin layer of myelin (left
789 panel). After treatment with IFB-088 (right panel), a subgroup of large calibre axons showed a
790 properly compacted (albeit still rather thin) myelin sheath. A side by side comparison of
791 myelination in two axons with similar calibre is shown in the lower panel.
792

Figure 7: IFB-088 treatment improves PMP22 stoichiometry in C3-PMP22 mice peripheral nerves and reduces ER stress. Evaluation of PMP22, P0 and BiP protein levels by WB in sciatic nerve protein lysates from WT mice treated with vehicle *b.i.d.* and C3-PMP22 (C3) mice treated with vehicle *b.i.d.* or IFB-088 at 0.5 or 1mg/kg *b.i.d.* (**a**) Representative picture. Three representative samples per condition out of five/six are shown. (**b**) Quantification of BiP protein level. (**c**) Quantification of the PMP22/P0 protein ratio. *P<0.05; **P<0.01; ****P<0.0001 by Student's T-test.

References

1 Anelli T, Sitia R (2008) Protein quality control in the early secretory pathway. The EMBO journal 27: 315-327 Doi 10.1038/sj.emboj.7601974

2 Avila RL, D'Antonio M, Bachi A, Inouye H, Feltri ML, Wrabetz L, Kirschner DA (2010) P0 (protein zero) mutation S34C underlies instability of internodal myelin in S63C mice. The Journal of biological chemistry 285: 42001-42012 Doi 10.1074/jbc.M110.166967

3 Bai Y, Ianokova E, Pu Q, Ghandour K, Levinson R, Martin JJ, Ceuterick-de Groote C, Mazanec R, Seeman P, Shy MEet al (2006) Effect of an R69C mutation in the myelin protein zero gene on myelination and ion channel subtypes. Archives of neurology 63: 1787-1794 Doi 10.1001/archneur.63.12.1787

4 Bai Y, Wu X, Brennan KM, Wang DS, D'Antonio M, Moran J, Svaren J, Shy ME (2018) Myelin protein zero mutations and the unfolded protein response in Charcot Marie Tooth disease type 1B. Ann Clin Transl Neurol 5: 445-455 Doi 10.1002/acn3.543

5 Biffi A, De Palma M, Quattrini A, Del Carro U, Amadio S, Visigalli I, Sessa M, Fasano S, Brambilla R, Marchesini Set al (2004) Correction of metachromatic leukodystrophy in the mouse model by transplantation of genetically modified hematopoietic stem cells. J Clin Invest 113: 1118-1129 Doi 10.1172/JCI19205

6 Boutary S, Caillaud M, El Madani M, Vallat JM, Loisel-Duwattez J, Rouyer A, Richard L, Gracia C, Urbinati G, Desmaele Det al (2021) Squalenoyl siRNA PMP22 nanoparticles are effective in treating mouse models of Charcot-Marie-Tooth disease type 1 A. Commun Biol 4: 317 Doi 10.1038/s42003-021-01839-2

7 Boutary S, Echaniz-Laguna A, Adams D, Loisel-Duwattez J, Schumacher M, Massaad C, Massaad-Massade L (2021) Treating PMP22 gene duplication-related Charcot-Marie-Tooth disease: the past, the present and the future. Translational research : the journal of laboratory and clinical medicine 227: 100-111 Doi 10.1016/j.trsl.2020.07.006

8 Chen Y, Kunjamma RB, Weiner M, Chan JR, Popko B (2021) Prolonging the integrated stress response enhances CNS remyelination in an inflammatory environment. Elife 10: Doi 10.7554/eLife.65469

9 Chen Y, Podojil JR, Kunjamma RB, Jones J, Weiner M, Lin W, Miller SD, Popko B (2019) Sephin1, which prolongs the integrated stress response, is a promising therapeutic for multiple sclerosis. Brain 142: 344-361 Doi 10.1093/brain/awy322

10 D'Antonio M, Michalovich D, Paterson M, Droggiti A, Woodhoo A, Mirsky R, Jessen KR (2006) Gene profiling and bioinformatic analysis of Schwann cell embryonic development and myelination. Glia 53: 501-515

11 D'Antonio M, Musner N, Scapin C, Ungaro D, Del Carro U, Ron D, Feltri ML, Wrabetz L (2013) Resetting translational homeostasis restores myelination in Charcot-Marie-Tooth disease type 1B mice. J Exp Med 210: 821-838 Doi 10.1084/jem.20122005

12 Das I, Krzyzosiak A, Schneider K, Wrabetz L, D'Antonio M, Barry N, Sigurdardottir A, Bertolotti A (2015) Preventing proteostasis diseases by selective inhibition of a phosphatase regulatory subunit. Science 348: 239-242 Doi 10.1126/science.aaa4484

13 Ellgaard L, Helenius A (2003) Quality control in the endoplasmic reticulum. Nature reviews Molecular cell biology 4: 181-191 Doi 10.1038/nrm1052

14 Ferri C, Quattrini A, D'Antonio M (2018) Electron Microscopy for the Analysis of Peripheral Nerve Myelin. Methods Mol Biol 1791: 3-13 Doi 10.1007/978-1-4939-7862-5_1

15 Fledrich R, Stassart RM, Sereda MW (2012) Murine therapeutic models for Charcot-Marie-Tooth (CMT) disease. British medical bulletin 102: 89-113 Doi 10.1093/bmb/lds010

16 Florio F, Ferri C, Scapin C, Feltri ML, Wrabetz L, D'Antonio M (2018) Sustained Expression of Negative Regulators of Myelination Protects Schwann Cells from Dysmyelination in a Charcot-Marie-Tooth 1B Mouse Model. The Journal of neuroscience : the official journal of the Society for Neuroscience 38: 4275-4287 Doi 10.1523/JNEUROSCI.0201-18.2018

17 Fortun J, Go JC, Li J, Amici SA, Dunn WA, Jr., Notterpek L (2006) Alterations in degradative pathways and protein aggregation in a neuropathy model based on PMP22 overexpression. Neurobiology of disease 22: 153-164 Doi 10.1016/j.nbd.2005.10.010

18 Fridman V, Bundy B, Reilly MM, Pareyson D, Bacon C, Burns J, Day J, Feely S, Finkel RS, Grider Tet al (2015) CMT subtypes and disease burden in patients enrolled in the Inherited Neuropathies Consortium natural history study: a cross-sectional analysis. Journal of neurology, neurosurgery, and psychiatry 86: 873-878 Doi 10.1136/jnnp-2014-308826

19 Gabriel JM, Erne B, Pareyson D, Sghirlanzoni A, Taroni F, Steck AJ (1997) Gene dosage effects in hereditary peripheral neuropathy. Expression of peripheral myelin protein 22 in Charcot-Marie-Tooth disease type 1A and hereditary neuropathy with liability to pressure palsies nerve biopsies. Neurology 49: 1635-1640

20 Gautier B, Hajjar H, Soares S, Berthelot J, Deck M, Abbou S, Campbell G, Ceprian M, Gonzalez S, Fovet CMet al (2021) AAV2/9-mediated silencing of PMP22 prevents the development of pathological features in a rat model of Charcot-Marie-Tooth disease 1 A. Nature communications 12: 2356 Doi 10.1038/s41467-021-22593-3

21 Grandis M, Vigo T, Passalacqua M, Jain M, Scazzola S, La Padula V, Brucal M, Benvenuto F, Nobbio L, Cadoni Aet al (2008) Different cellular and molecular mechanisms for early and late-onset myelin protein zero mutations. Human molecular genetics 17: 1877-1889 Doi 10.1093/hmg/ddn083

22 Greenfield S, Brostoff S, Eylar EH, Morell P (1973) Protein composition of myelin of the peripheral nervous system. Journal of neurochemistry 20: 1207-1216.

23 Ha N, Choi YI, Jung N, Song JY, Bae DK, Kim MC, Lee YJ, Song H, Kwak G, Jeong Set al (2020) A novel histone deacetylase 6 inhibitor improves myelination of Schwann cells in a model of Charcot-Marie-Tooth disease type 1A. British journal of pharmacology 177: 5096-5113 Doi 10.1111/bph.15231

24 Hantke J, Carty L, Wagstaff LJ, Turmaine M, Wilton DK, Quintes S, Koltzenburg M, Baas F, Mirsky R, Jessen KR (2014) c-Jun activation in Schwann cells protects against loss of sensory axons in inherited neuropathy. Brain 137: 2922-2937 Doi 10.1093/brain/awu257

25 Harding HP, Zhang Y, Bertolotti A, Zeng H, Ron D (2000) Perk is essential for translational regulation and cell survival during the unfolded protein response. Mol Cell 5: 897-904

26 Hayasaka K, Ohnishi A, Takada G, Fukushima Y, Murai Y (1993) Mutation of the myelin P0 gene in Charcot-Marie-tooth neuropathy type 1. Biochemical and biophysical research communications 194: 1317-1322 Doi S0006291X83719686

27 Hirt N, Eggermann K, Hyrenbach S, Lambeck J, Busche A, Fischer J, Rudnik-Schoneborn S, Gaspar H (2015) Genetic dosage compensation via co-occurrence of PMP22 duplication and PMP22 deletion. Neurology 84: 1605-1606 Doi 10.1212/WNL.0000000000001470

28 Howard P, Feely SME, Grider T, Bacha A, Scarlato M, Fazio R, Quattrini A, Shy ME, Previtali SC (2021) Loss of Function MPZ Mutation causes milder CMT1B Neuropathy. Journal of the peripheral nervous system : JPNS: Doi 10.1111/jns.12452

29 Huxley C, Passage E, Manson A, Putzu G, Figarella-Branger D, Pellissier JF, Fontes M (1996) Construction of a mouse model of Charcot-Marie-Tooth disease type 1A by pronuclear injection of human YAC DNA. Human molecular genetics 5: 563-569 Doi 5d0403

30 Huxley C, Passage E, Robertson AM, Youl B, Huston S, Manson A, Saberan-Djoniedi D, Figarella-Branger D, Pellissier JF, Thomas PKet al (1998) Correlation between varying levels of PMP22 expression and the degree of demyelination and reduction in nerve conduction velocity in transgenic mice. Human molecular genetics 7: 449-458

31 Katona I, Wu X, Feely SM, Sottile S, Siskind CE, Miller LJ, Shy ME, Li J (2009) PMP22 expression in dermal nerve myelin from patients with CMT1A. Brain 132: 1734-1740 Doi 10.1093/brain/awp113

32 Khajavi M, Inoue K, Wiszniewski W, Ohyama T, Snipes GJ, Lupski JR (2005) Curcumin treatment abrogates endoplasmic reticulum retention and aggregation-induced apoptosis associated with neuropathy-causing myelin protein zero-truncating mutants. American journal of human genetics 77: 841-850 Doi 10.1086/497541

33 Khajavi M, Shiga K, Wiszniewski W, He F, Shaw CA, Yan J, Wensel TG, Snipes GJ, Lupski JR (2007) Oral curcumin mitigates the clinical and neuropathologic phenotype of the Trembler-J mouse: a potential therapy for inherited neuropathy. American journal of human genetics 81: 438-453 Doi 10.1086/519926

913 34 Kimura J (2005) Nerve conduction and electromyography. In: Dyck P.J., Thomas PK (eds)
914 Peripheral Neuropathy. Elsevier/Saunders, City, pp 899-970
915 35 Lee S, Bazick H, Chittoor-Vinod V, Al Salihi MO, Xia G, Notterpek L (2018) Elevated
916 Peripheral Myelin Protein 22, Reduced Mitotic Potential, and Proteasome Impairment in
917 Dermal Fibroblasts from Charcot-Marie-Tooth Disease Type 1A Patients. The American
918 journal of pathology 188: 728-738 Doi 10.1016/j.ajpath.2017.10.021
919 36 Lemke G, Axel R (1985) Isolation and sequence of a cDNA encoding the major structural
920 protein of peripheral myelin. Cell 40: 501-508.
921 37 Li J, Bai Y, Ghandour K, Qin P, Grandis M, Trostinskaia A, Ianakova E, Wu X, Schenone A,
922 Vallat JMet al (2005) Skin biopsies in myelin-related neuropathies: bringing molecular
923 pathology to the bedside. Brain 128: 1168-1177.
924 38 Lin JH, Li H, Zhang Y, Ron D, Walter P (2009) Divergent effects of PERK and IRE1 signaling
925 on cell viability. PloS one 4: e4170 Doi 10.1371/journal.pone.0004170
926 39 Lupski JR, de Oca-Luna RM, Slaugenhaupt S, Pentao L, Guzzetta V, Trask BJ, Saucedo-
927 Cardenas O, Barker DF, Killian JM, Garcia CAet al (1991) DNA duplication associated with
928 Charcot-Marie-Tooth disease type 1A. Cell 66: 219-232 Doi 0092-8674(91)90613-4
929 40 Marinko JT, Carter BD, Sanders CR (2020) Direct relationship between increased
930 expression and mistrafficking of the Charcot-Marie-Tooth-associated protein PMP22.
931 The Journal of biological chemistry 295: 11963-11970 Doi 10.1074/jbc.AC120.014940
932 41 Miller LJ, Patzko A, Lewis RA, Shy ME (2012) Phenotypic presentation of the Ser63Del
933 MPZ mutation. Journal of the peripheral nervous system : JPNS 17: 197-200 Doi
934 10.1111/j.1529-8027.2012.00398.x
935 42 Monk KR, Feltri ML, Taveggia C (2015) New insights on Schwann cell development. Glia
936 63: 1376-1393 Doi 10.1002/glia.22852
937 43 Murphy SM, Laura M, Fawcett K, Pandraud A, Liu YT, Davidson GL, Rossor AM, Polke JM,
938 Castleman V, Manji Het al (2012) Charcot-Marie-Tooth disease: frequency of genetic
939 subtypes and guidelines for genetic testing. Journal of neurology, neurosurgery, and
940 psychiatry 83: 706-710 Doi 10.1136/jnnp-2012-302451
941 44 Nave KA (2010) Myelination and support of axonal integrity by glia. Nature 468: 244-252
942 Doi 10.1038/nature09614
943 45 Notterpek L, Ryan MC, Tobler AR, Shooter EM (1999) PMP22 accumulation in
944 aggresomes: implications for CMT1A pathology. Neurobiology of disease 6: 450-460 Doi
945 10.1006/nbdi.1999.0274
946 46 Okamoto Y, Pehlivan D, Wiszniewski W, Beck CR, Snipes GJ, Lupski JR, Khajavi M (2013)
947 Curcumin facilitates a transitory cellular stress response in Trembler-J mice. Human
948 molecular genetics 22: 4698-4705 Doi 10.1093/hmg/ddt318
949 47 Pantera H, Shy ME, Svaren J (2020) Regulating PMP22 expression as a dosage sensitive
950 neuropathy gene. Brain research 1726: 146491 Doi 10.1016/j.brainres.2019.146491
951 48 Pareek S, Notterpek L, Snipes GJ, Naef R, Sossin W, Laliberte J, Iacampo S, Suter U,
952 Shooter EM, Murphy RA (1997) Neurons promote the translocation of peripheral myelin
953 protein 22 into myelin. The Journal of neuroscience : the official journal of the Society
954 for Neuroscience 17: 7754-7762.

49 Pareek S, Suter U, Snipes GJ, Welcher AA, Shooter EM, Murphy RA (1993) Detection and processing of peripheral myelin protein PMP22 in cultured Schwann cells. The Journal of biological chemistry 268: 10372-10379

50 Parkinson DB, Bhaskaran A, Arthur-Farraj P, Noon LA, Woodhoo A, Lloyd AC, Feltri ML, Wrabetz L, Behrens A, Mirsky Ret al (2008) c-Jun is a negative regulator of myelination. The Journal of cell biology 181: 625-637 Doi 10.1083/jcb.200803013

51 Passage E, Norreel JC, Noack-Fraissignes P, Sanguedolce V, Pizant J, Thirion X, Robaglia-Schlupp A, Pellissier JF, Fontes M (2004) Ascorbic acid treatment corrects the phenotype of a mouse model of Charcot-Marie-Tooth disease. Nature medicine 10: 396-401 Doi 10.1038/nm1023

52 Patzko A, Bai Y, Saporta MA, Katona I, Wu X, Vizzuso D, Feltri ML, Wang S, Dillon LM, Kamholz Jet al (2012) Curcumin derivatives promote Schwann cell differentiation and improve neuropathy in R98C CMT1B mice. Brain 135: 3551-3566 Doi 10.1093/brain/aws299

53 Pennuto M, Tinelli E, Malaguti M, Del Carro U, D'Antonio M, Ron D, Quattrini A, Feltri ML, Wrabetz L (2008) Ablation of the UPR-Mediator CHOP Restores Motor Function and Reduces Demyelination in Charcot-Marie-Tooth 1B Mice. Neuron 57: 393-405 Doi 10.1016/j.neuron.2007.12.021

54 Perea J, Robertson A, Tolmachova T, Muddle J, King RH, Ponsford S, Thomas PK, Huxley C (2001) Induced myelination and demyelination in a conditional mouse model of Charcot-Marie-Tooth disease type 1A. Human molecular genetics 10: 1007-1018

55 Sanmaneechai O, Feely S, Scherer SS, Herrmann DN, Burns J, Muntoni F, Li J, Siskind CE, Day JW, Laura Met al (2015) Genotype-phenotype characteristics and baseline natural history of heritable neuropathies caused by mutations in the MPZ gene. Brain 138: 3180-3192 Doi 10.1093/brain/awv241

56 Saporta MA, Shy BR, Patzko A, Bai Y, Pennuto M, Ferri C, Tinelli E, Saveri P, Kirschner D, Crowther Met al (2012) MpzR98C arrests Schwann cell development in a mouse model of early-onset Charcot-Marie-Tooth disease type 1B. Brain 135: 2032-2047 Doi 10.1093/brain/aws140

57 Schlebach JP, Peng D, Kroncke BM, Mittendorf KF, Narayan M, Carter BD, Sanders CR (2013) Reversible folding of human peripheral myelin protein 22, a tetraspan membrane protein. Biochemistry 52: 3229-3241 Doi 10.1021/bi301635f

58 Sereda M, Griffiths I, Puhlhofer A, Stewart H, Rossner MJ, Zimmerman F, Magyar JP, Schneider A, Hund E, Meinck HMet al (1996) A transgenic rat model of Charcot-Marie-Tooth disease. Neuron 16: 1049-1060

59 Shapiro L, Doyle JP, Hensley P, Colman DR, Hendrickson WA (1996) Crystal structure of the extracellular domain from P0, the major structural protein of peripheral nerve myelin. Neuron 17: 435-449.

60 Skre H (1974) Genetic and clinical aspects of Charcot-Marie-Tooth's disease. Clinical genetics 6: 98-118

61 Takeo T, Nakagata N (2011) Reduced glutathione enhances fertility of frozen/thawed C57BL/6 mouse sperm after exposure to methyl-beta-cyclodextrin. Biology of reproduction 85: 1066-1072 Doi 10.1095/biolreprod.111.092536

62 Taveggia C, Zanazzi G, Petrylak A, Yano H, Rosenbluth J, Einheber S, Xu X, Esper RM, Loeb JA, Shrager Pet al (2005) Neuregulin-1 type III determines the ensheathment fate of axons. Neuron 47: 681-694 Doi 10.1016/j.neuron.2005.08.017

63 Timmerman V, Nelis E, Van Hul W, Nieuwenhuijsen BW, Chen KL, Wang S, Ben Othman K, Cullen B, Leach RJ, Hanemann COet al (1992) The peripheral myelin protein gene PMP-22 is contained within the Charcot-Marie-Tooth disease type 1A duplication. Nature genetics 1: 171-175 Doi 10.1038/ng0692-171

64 Vallat JM, Sindou P, Preux PM, Tabaraud F, Milor AM, Couratier P, LeGuern E, Brice A (1996) Ultrastructural PMP22 expression in inherited demyelinating neuropathies. Annals of neurology 39: 813-817.

65 Verhamme C, King RH, ten Asbroek AL, Muddle JR, Nourallah M, Wolterman R, Baas F, van Schaik IN (2011) Myelin and axon pathology in a long-term study of PMP22-overexpressing mice. Journal of neuropathology and experimental neurology 70: 386-398 Doi 10.1097/NEN.0b013e318217eba0

66 VerPlank JJS, Gawron J, Silvestri NJ, Feltri ML, Wrabetz L, Goldberg AL (2021) Raising cGMP restores proteasome function and myelination in mice with a proteotoxic neuropathy. Brain: Doi 10.1093/brain/awab249

67 VerPlank JJS, Lokireddy S, Feltri ML, Goldberg AL, Wrabetz L (2018) Impairment of protein degradation and proteasome function in hereditary neuropathies. Glia 66: 379-395 Doi 10.1002/glia.23251

68 Volpi VG, Ferri C, Fregno I, Del Carro U, Bianchi F, Scapin C, Pettinato E, Solda T, Feltri ML, Molinari Met al (2019) Schwann cells ER-associated degradation contributes to myelin maintenance in adult nerves and limits demyelination in CMT1B mice. PLoS genetics 15: e1008069 Doi 10.1371/journal.pgen.1008069

69 Volpi VG, Touvier T, D'Antonio M (2017) Endoplasmic Reticulum Protein Quality Control Failure in Myelin Disorders. Front Mol Neurosci 9: 162 Doi 10.3389/fnmol.2016.00162

70 Wrabetz L, D'Antonio M, Pennuto M, Dati G, Tinelli E, Fratta P, Previtali S, Imperiale D, Zielasek J, Toyka Ket al (2006) Different intracellular pathomechanisms produce diverse Myelin Protein Zero neuropathies in transgenic mice. The Journal of neuroscience : the official journal of the Society for Neuroscience 26: 2358-2368 Doi 10.1523/JNEUROSCI.3819-05.2006

71 Wrabetz L, Feltri ML, Quattrini A, Imperiale D, Previtali S, D'Antonio M, Martini R, Yin X, Trapp BD, Zhou Let al (2000) P(0) glycoprotein overexpression causes congenital hypomyelination of peripheral nerves. J Cell Biol 148: 1021-1034

72 Wu S, Stone S, Yue Y, Lin W (2021) Endoplasmic reticulum associated degradation is required for maintaining endoplasmic reticulum homeostasis and viability of mature Schwann cells in adults. Glia 69: 489-506 Doi 10.1002/glia.23910

73 Zhao HT, Damle S, Ikeda-Lee K, Kuntz S, Li J, Mohan A, Kim A, Hung G, Scheideler MA, Scherer SSet al (2018) PMP22 antisense oligonucleotides reverse Charcot-Marie-Tooth disease type 1A features in rodent models. The Journal of clinical investigation 128: 359-368 Doi 10.1172/JCI96499

1040

1041

1042

1043

1044

1045

1046

1047

1048

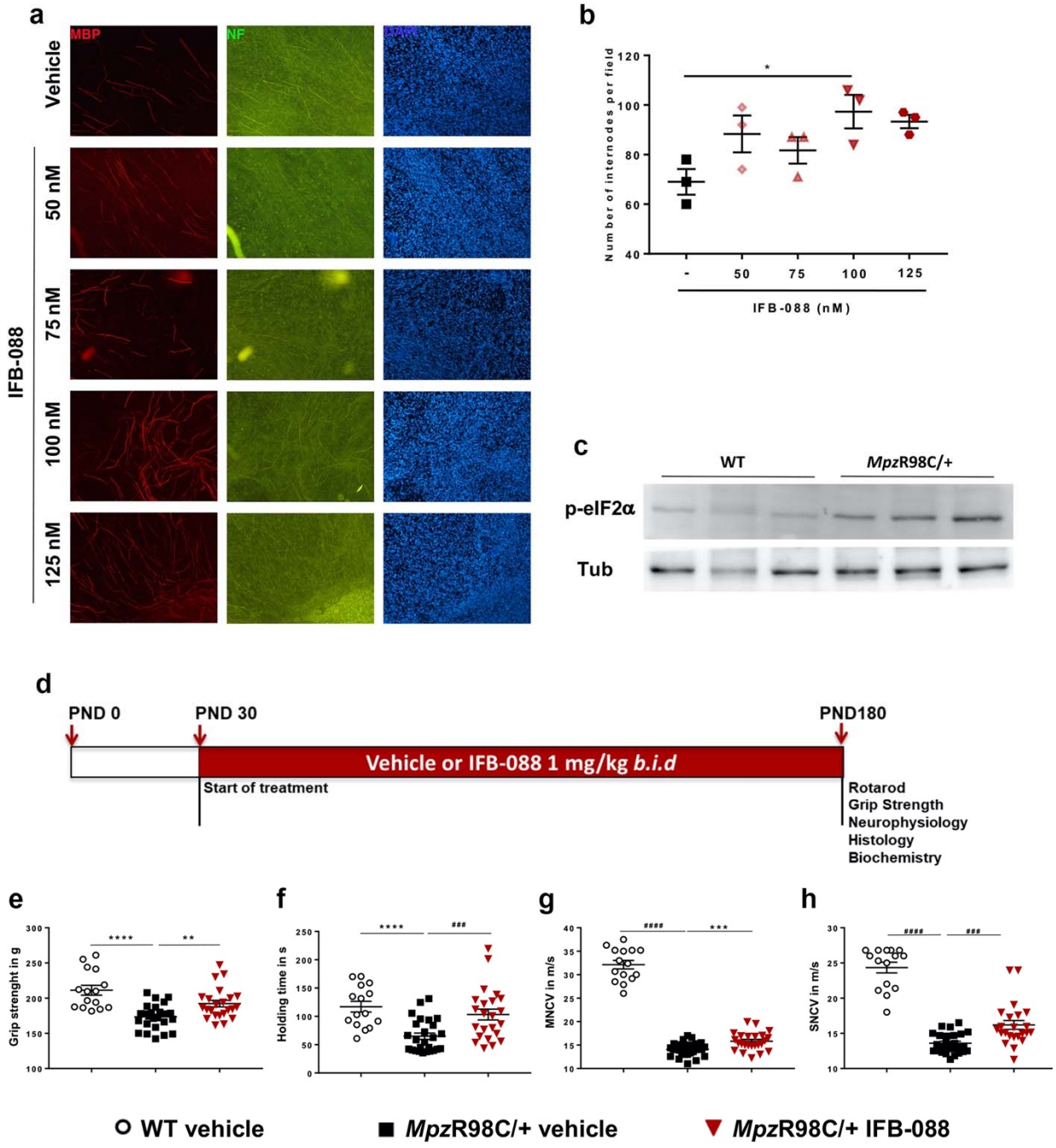

Figure 1

1054

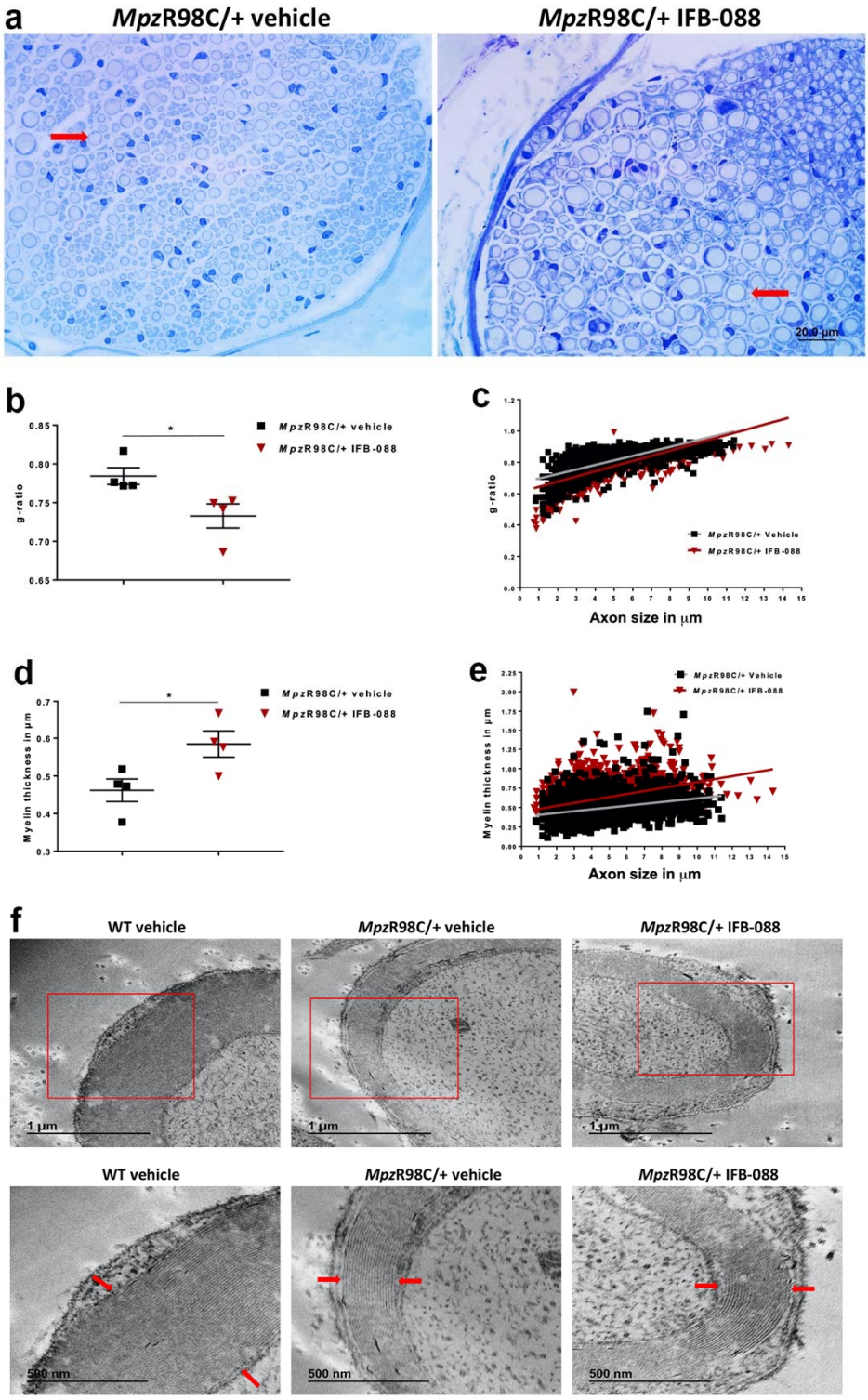

Figure 2

1055

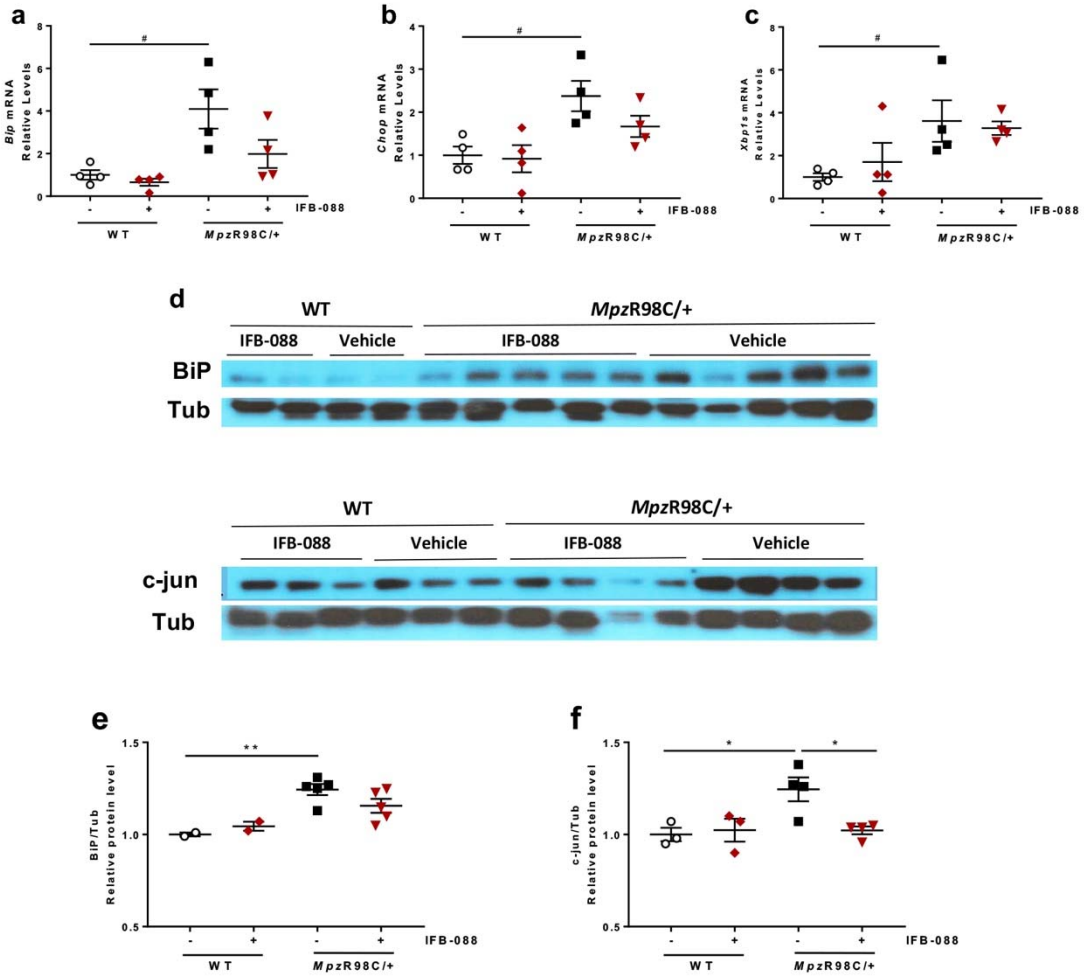

Figure 3

1066

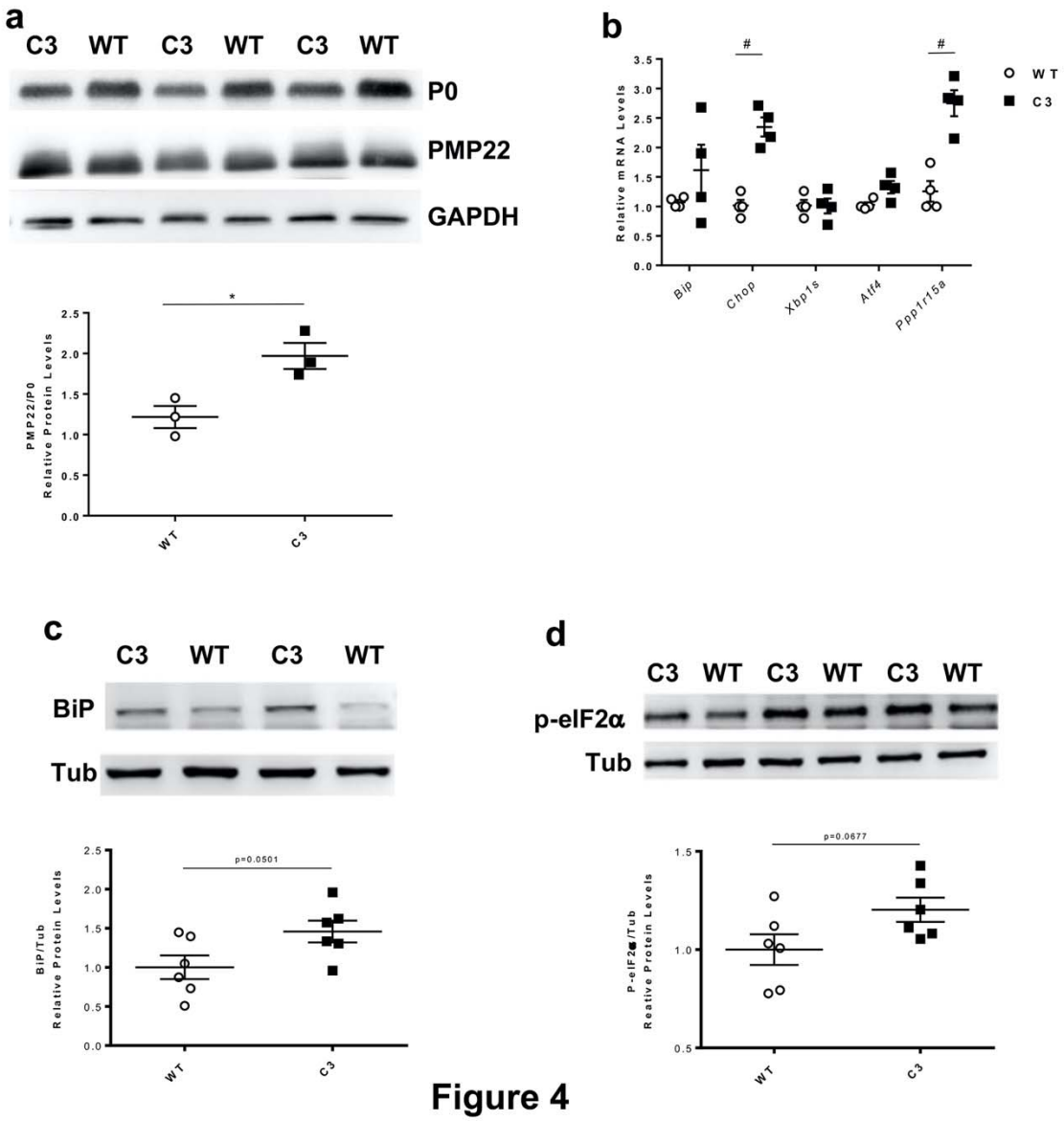

Figure 4

1067

1068

1069

1070

1071

1072

1073

1074

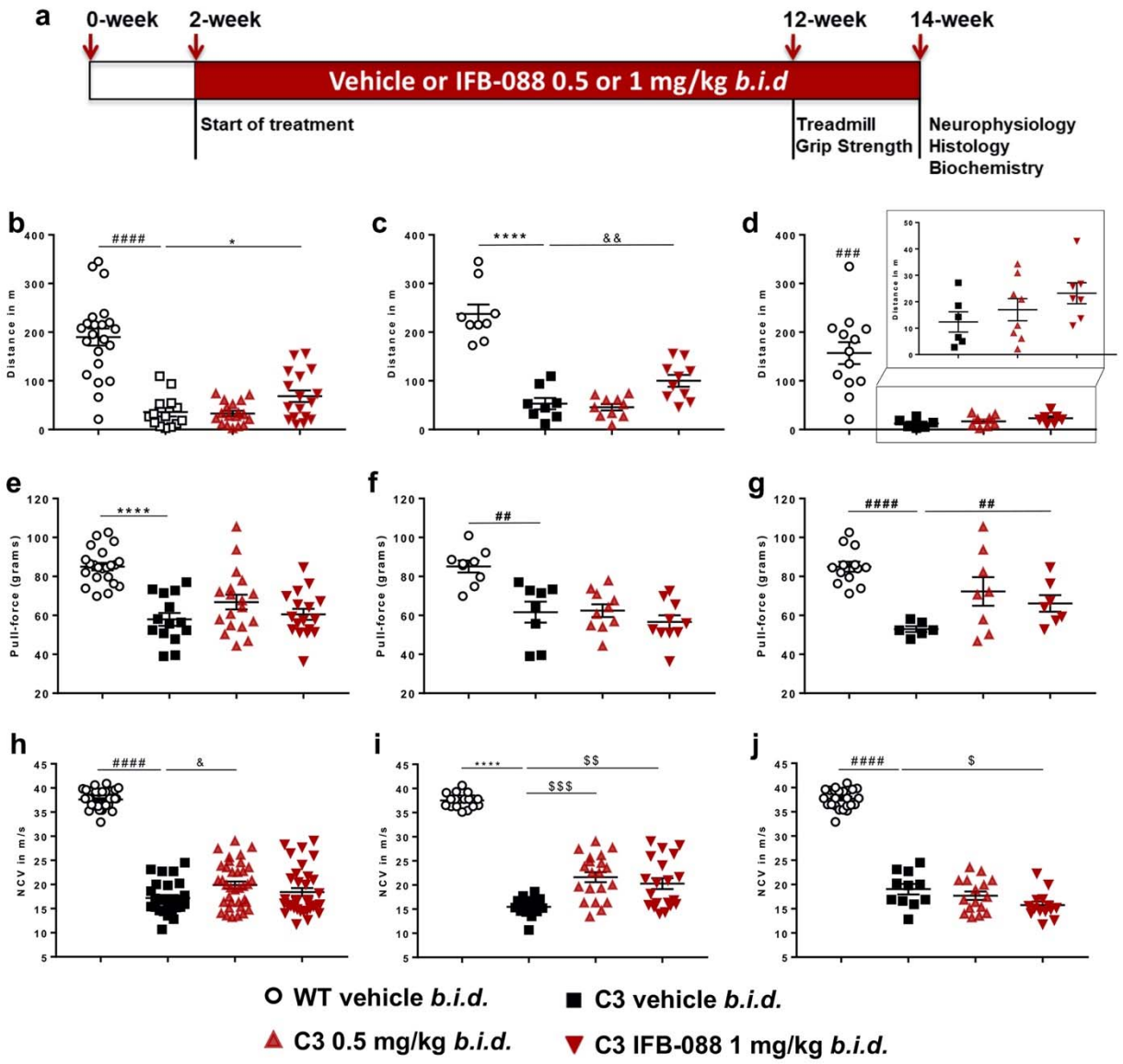

Figure 5

1075

1076

1077

1078

1079

1080

1081

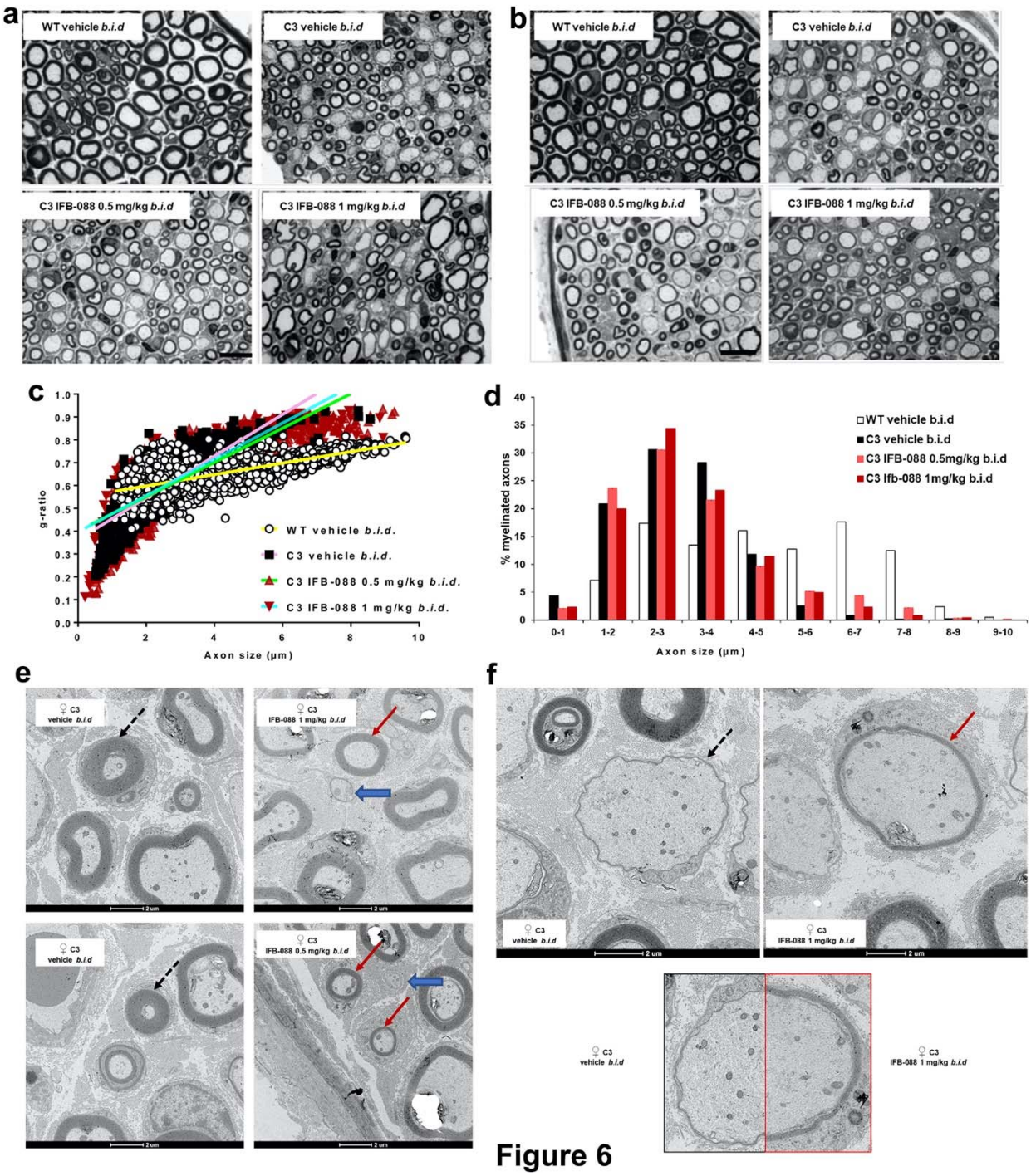

Figure 6

1087

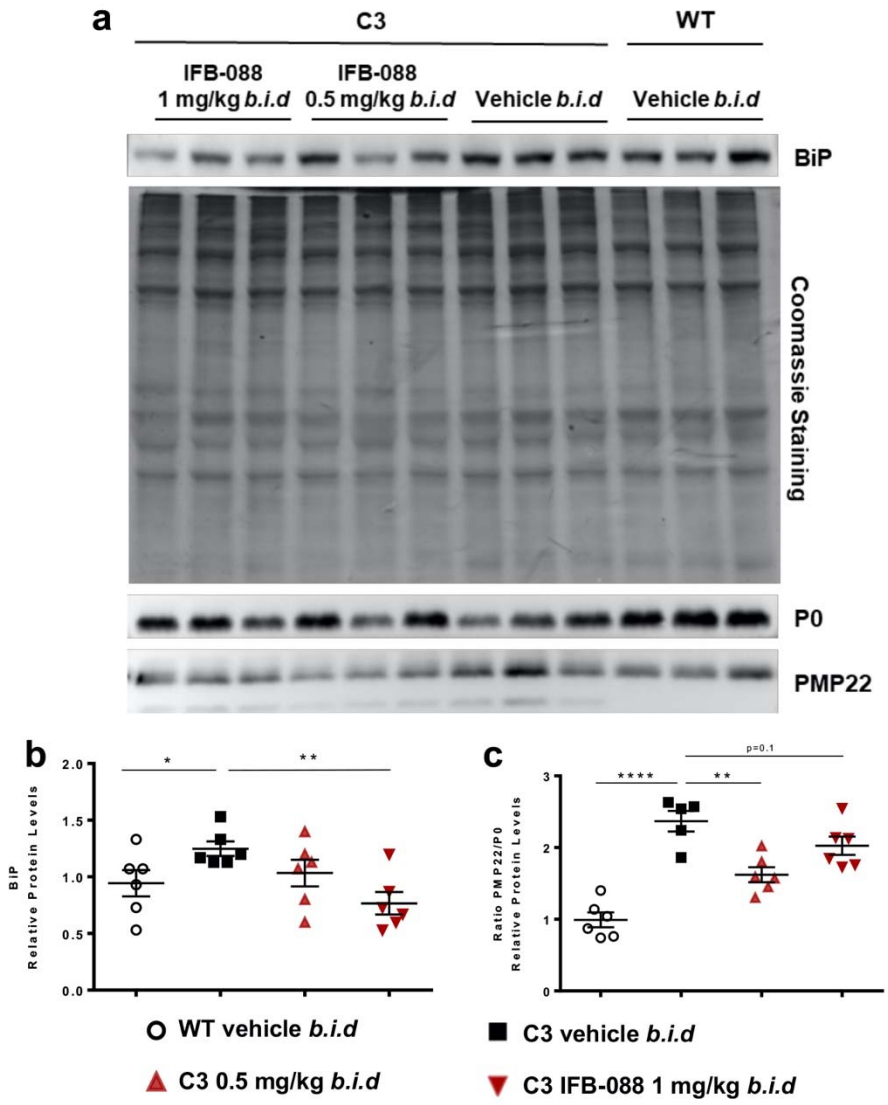

Figure 7

1088